ORIGINAL ARTICLE OPEN ACCESS

Multiple Reflections on Huygens' Principle

Kees Wapenaar 🆔

Department of Geoscience and Engineering, Delft University of Technology, Delft, The Netherlands

Correspondence: Kees Wapenaar (c.p.a.wapenaar@tudelft.nl)

ABSTRACT

According to Huygens' principle, all points on a wave front act as secondary sources emitting spherical waves and the envelope of these spherical waves forms a new wave front. In the mathematical formulation of Huygens' principle, the waves emitted by the secondary sources are represented by Green's functions. In many present-day applications of Huygens' principle, these Green's functions are replaced by their time-reversed versions, thus forming a basis for backpropagation, imaging, inversion, seismic interferometry, etc. However, when the input wave field is available only on a single open boundary, this approach has its limitations. In particular, it does not properly account for multiply reflected waves. This is remedied by a modified form of Huygens' principle, in which the Green's functions are replaced by focusing functions. The modified Huygens' principle forms a basis for imaging, inverse scattering, monitoring of induced sources, etc., thereby properly taking multiply reflected waves into account.

1 | Introduction

Dutch mathematician, physicist and astronomer Christiaan Huygens (1629–1695) described light as a longitudinal mechanical wave, propagating through an ether medium. Even though, centuries later, Maxwell proposed light as a transverse electromagnetic wave and Einstein showed that it does not need an ether to support its propagation, the early wave theoretical approach of Huygens appeared very effective in the analysis of the propagation and reflection of light. In his book *Traité de la Lumière* (Treatise on Light, published in 1690), he explains that around each undulating particle of the matter through which a wave propagates, a spherical wave is formed of which this particle is the centre. The common tangent (or envelope) of these spherical waves forms a new wave front. This is, in a nutshell, Huygens' principle, and it applies to light as well as to other wave phenomena. For an extensive discussion of the work of Huygens and his important role in bridging ancient and modern science, see Moser and Robinson (2024).

In the early nineteenth century, French physicist Augustin-Jean Fresnel (1788–1827) added the theory of interference to Huygens' principle. With this extension, the new wave front along the envelope of aforementioned spherical waves can be explained as the result of constructive interference of these spherical waves. In the following, when we speak of 'Huygens' principle', we mean the original theory of Huygens, extended with the theory of interference.

Figure 1 is an illustration of Huygens' principle, applied to acoustic waves. A point source, indicated by the red star, emits a circular wave which propagates through a medium with a constant propagation velocity (the example is in two dimensions; hence, instead of spherical waves, we have circular waves). At a certain time, this wave reaches a screen with a small opening (Figure 1a). The wave field in this opening acts as a secondary source, which emits a circular wave into the half-space above the screen. Figure 1b shows a similar setup, but this time the screen has many small openings, which all act as secondary sources,
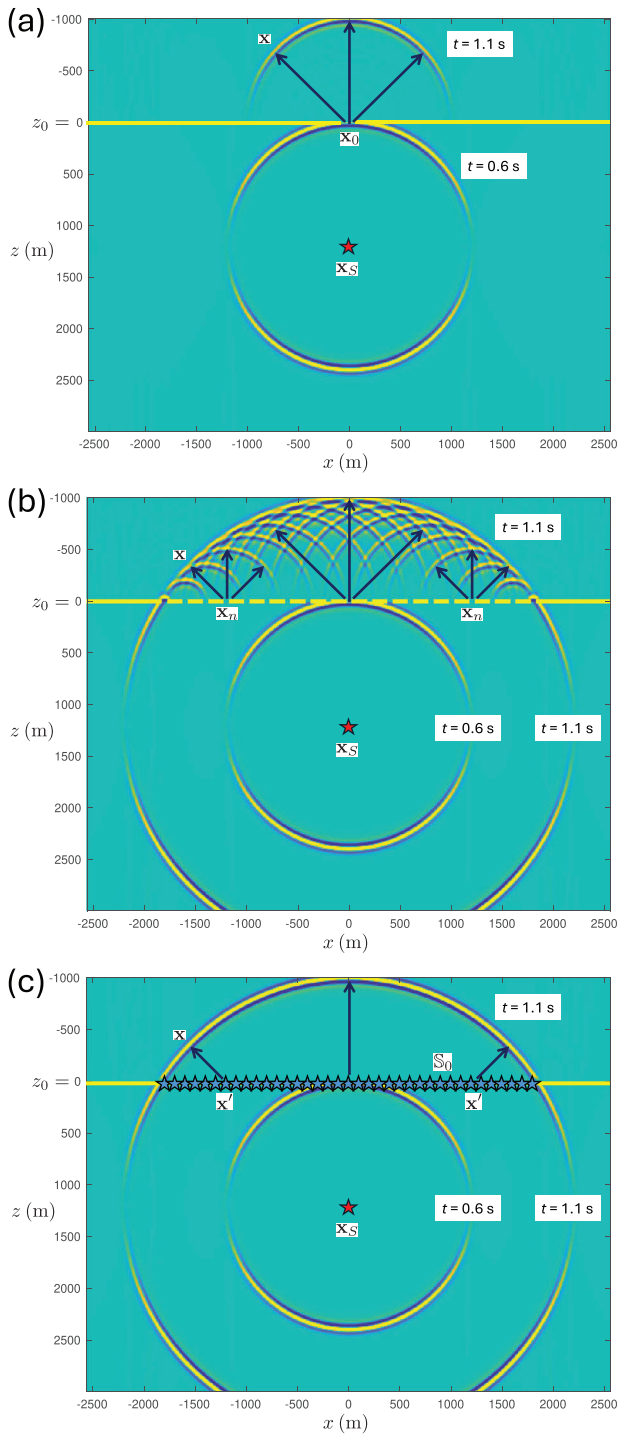
Figure 1 | Illustration of Huygens' principle for acoustic waves in a homogeneous medium. (a) A source at $\mathbf{x}_S$ emits a circular wave. The wave field in the opening of the screen at $\mathbf{x}_0$ acts as a secondary source, emitting a secondary circular wave into the upper half-space. (b) Many openings in the screen, acting as secondary sources. The envelope of the superposition of the secondary circular waves in the upper half-space approaches the circular wave, originating from the source at $\mathbf{x}_S$. (c) All points in one large opening in the screen act as secondary sources (indicated by the blue stars). The superposition of the secondary circular waves in the upper half-space has converged to the circular wave, originating from the source at $\mathbf{x}_S$. Animations of this and other figures are available. For details, see the Data Availability Statement.

emitting circular waves at the time the original wave reaches these openings. Hence, the field above the screen consists of a superposition of circular waves. The envelope of these superposed waves approximately forms a circular wave, resembling the wave that would be radiated by the original point source into the upper half-space in the absence of the screen. In Figure 1c, the screen contains one large opening. All points in this opening act as secondary sources (indicated by the dense distribution of blue stars), and the superposition of the circular waves above the screen has indeed converged to the circular wave radiated by the original source.

Huygens' principle has found many applications in optics, acoustics and other fields in which wave propagation and scattering play a role. In this paper, we restrict ourselves to applications in acoustics and geophysics, in particular for wave field extrapolation. Traditionally, the waves emitted by the secondary sources in Huygens' principle are represented by Green's functions. In Section 2, we review applications of Huygens' principle in forward and inverse wave field extrapolation through homogeneous and inhomogeneous media. It appears that with the traditional Huygens' principle, internal multiply reflected waves are not correctly handled in inverse extrapolation through an inhomogeneous medium. In Section 3, we first introduce focusing functions for homogeneous and inhomogeneous media. Next, we discuss a modified version of Huygens' principle, in which the Green's functions are replaced by these focusing functions. We discuss applications of this modified Huygens' principle in forward and inverse wave field extrapolation through an inhomogeneous medium and in the retrieval of the homogeneous Green's function of an inhomogeneous medium. We show that internal multiply reflected waves are correctly handled in these applications.

The style of the main text is informal, with an emphasis on explanations of the different forms of Huygens' principle, using simple mathematics. More detailed derivations can be found in the Appendices.

2 | Traditional Huygens' Principle, Using Green's Functions

2.1 | Forward Wave Field Extrapolation Through a Homogeneous Medium

We discuss some mathematics behind Huygens' principle, as illustrated in Figure 1, and use this as a starting point for the discussion of forward wave field extrapolation. We define a Cartesian coordinate system, with the z-axis pointing downward and the coordinate vector $\mathbf{x}$ denoting position in this system. For the three-dimensional (3D) situation, this vector is defined as $\mathbf{x} = (x, y, z)$; whereas most of the theory in this paper holds for three dimensions, the examples are in two dimensions, in which case the coordinate vector is defined as $\mathbf{x} = (x, z)$. Time is denoted by t.

Let $\mathbf{x}_S$ denote the position of a monopole source (in Figure 1 it is defined as $\mathbf{x}_S = (0, 1200)$ m). We define the acoustic Green's function $G(\mathbf{x}, \mathbf{x}_S, t)$ (named after George Green, 1793–1841) as the response to an impulsive monopole source at $\mathbf{x}_S$ and $t = 0$,

observed at $\mathbf{x}$ as a function of t. The Green's function is a causal function of time, meaning $G(\mathbf{x}, \mathbf{x}_S, t) = 0$ for $t < 0$. The source of the Green's function is a volume-injection rate source (see Appendix A1 for further details). When the source function in an actual situation is not an impulse but a transient wavelet $s(t)$, then the observed acoustic pressure is given by the convolution of the Green's function with the wavelet, according to

$$p(\mathbf{x}, t) = \int_0^\infty G(\mathbf{x}, \mathbf{x}_S, t') s(t - t') \mathrm{d}t'. \tag{1}$$

To simplify the notation, here and in subsequent sections, we introduce the convolutional symbol $*$ and replace the integral notation of Equation (1) by

$$p(\mathbf{x}, t) = G(\mathbf{x}, \mathbf{x}_S, t) * s(t). \tag{2}$$

The wave fronts in Figure 1 below the screen are described by this equation. The source function $s(t)$ is a Ricker wavelet with a central frequency of 20 Hz, and $G(\mathbf{x}, \mathbf{x}_S, t)$ is the two-dimensional (2D) Green's function in a homogeneous lossless medium with propagation velocity $c = 2000$ m/s and mass density $\rho = 1000$ kg/m^3 (hence, the wavelength at the central frequency is 100 m). The amplitudes along the wave fronts are tapered at large propagation angles (relative to the vertical axis), and waves reflected by the screen are not shown. Let $\mathbf{x}_0 = (x_0, z_0)$ denote the position of the opening in the screen in Figure 1a, with z_0 being the depth level of the screen (with $z_0 = 0$ m here and in subsequent figures). According to Huygens' principle, the acoustic pressure at this position, $p(\mathbf{x}_0, t)$, acts as a secondary source for the wave field above the screen; hence, analogous to Equation (2), this is given by

$$p(\mathbf{x}, t) \propto G(\mathbf{x}, \mathbf{x}_0, t) * p(\mathbf{x}_0, t), \tag{3}$$

where the symbol $\propto$ means 'proportional to'. Next, let $\mathbf{x}_n = (n\Delta x, z_0)$, $n = -N, \dots, -1, 0, 1, \dots, N$, denote the positions of the openings in the screen in Figure 1b (with $N = 9$ and $\Delta x = 200$ m). Then, according to Huygens' superposition principle, the wave field in the half-space above the screen can be expressed as

$$p(\mathbf{x}, t) \propto \sum_{n=-N}^{N} G(\mathbf{x}, \mathbf{x}_n, t) * p(\mathbf{x}_n, t). \tag{4}$$

Next, for the situation of one large opening in the screen, as in Figure 1c, we reduce the distance between the secondary sources to $\Delta x = 10$ m. Since this is significantly smaller than the central wavelength of 100 m, we now have effectively a continuum of secondary sources and we replace the summation by an integration, according to

$$p(\mathbf{x}, t) \propto \int_{\mathbb{S}_0} G(\mathbf{x}, \mathbf{x}', t) * p(\mathbf{x}', t) \mathrm{d}\mathbf{x}', \tag{5}$$

where $\mathbb{S}_0$ denotes the integration boundary (the opening in the screen as in Figure 1c, or an infinite horizontal boundary in the absence of the screen). For the 2D situation considered here, this is a 1D integral over x'; for the 3D situation, it is a 2D integral over x' and y'. In both cases, z' is fixed and equal to z_0, being the depth of integration boundary $\mathbb{S}_0$.
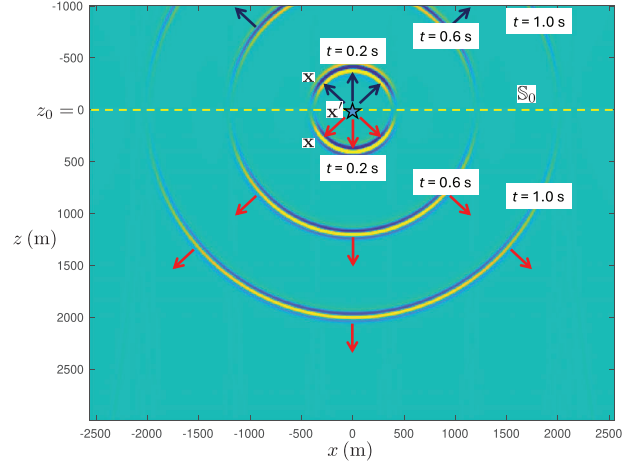

Figure 2 | Dipole Green's function $G_\mathrm{d}(\mathbf{x}, \mathbf{x}', t)$ (convolved with a Ricker wavelet to get a nicer display) in a homogeneous medium, for a dipole at $\mathbf{x}'$ on $\mathbb{S}_0$ at depth z_0. In the mathematical formulation of Huygens' principle, this dipole Green's function describes the propagation from a secondary source at $\mathbf{x}'$ to an observation point $\mathbf{x}$ (see Equation 6).

Up to this point, we captured the physical arguments of Huygens and Fresnel in mathematical form. Using only physical arguments, the proportionality factor remains unknown. In the 19th century, Kirchhoff, Helmholtz, Rayleigh and others derived expressions which formalize Huygens' principle. In Appendix B, we summarize their derivation and obtain the following more precise form of Equation (5)

$$p(\mathbf{x}, t) = -2 \int_{\mathbb{S}_0} G_\mathrm{d}(\mathbf{x}, \mathbf{x}', t) * p(\mathbf{x}', t) \mathrm{d}\mathbf{x}', \tag{6}$$

for $\mathbf{x}$ above $\mathbb{S}_0$. Here, $G_\mathrm{d}(\mathbf{x}, \mathbf{x}', t)$ is the response, observed at $\mathbf{x}$ and t, to an impulsive dipole source at $\mathbf{x}'$ and $t = 0$, with $\mathbf{x}'$ on $\mathbb{S}_0$; see Figure 2 (actually we already used this dipole Green's function in generating the example in Figure 1). This dipole Green's function is further specified in Appendix A3. The minus sign in Equation (6) stems from the definition of the dipole (it is oriented with respect to the positive z-axis, whereas in Equation (6) it radiates in the negative z-direction). The factor 2 in Equation (6) is explained later.

Huygens' wave-theoretical description of light was not immediately accepted. One of the reasons was that it does not explain why the secondary sources radiate only forward: if each point in a wave field acts as a secondary source, one would expect it to radiate in all directions (like the dipole source of the Green's function in Figure 2). Consequently, the envelope of the superposed waves of all secondary sources on a plane would consist of two contributions: one propagating forward, in the direction of the original wave, and one propagating backward, against the direction of the original wave. In the time of Huygens, it was not clear why the secondary sources do not give rise to this backward propagating wave. This was seen as a serious drawback of Huygens' wave-theoretical approach. Newton's competing theory (light consisting of particles moving along straight lines) did not have this drawback, but it had other shortcomings, such as not explaining diffraction and interference. All in all, Huygens' wave theory has withstood the test of time.

To understand why the secondary sources generate only the forward propagating wave, consider the Kirchhoff–Helmholtz integral in Equation (B8). This integral contains monopole and dipole Green's functions, driven by the particle velocity and acoustic pressure, respectively, at the horizontal boundary $\mathbb{S}_0$. Equation (B8) states that the combination of secondary monopole and dipole responses yields the forward propagating wave in the half-space above $\mathbb{S}_0$, whereas their contributions cancel in the half-space below $\mathbb{S}_0$. Moreover, for the homogeneous medium configuration of Figure 1, the secondary monopoles and dipoles give equal contributions to the wave field above $\mathbb{S}_0$, so one of the terms can be omitted and the other term doubled, yielding Equation (6) and explaining the factor 2 in this equation. Whereas Equation (B8) holds for $\mathbf{x}$ at either side of $\mathbb{S}_0$, Equation (6) is only valid for $\mathbf{x}$ above $\mathbb{S}_0$.

Huygens' principle was developed in the pre-Industrial age. At the time, it was merely meant to explain the physics of wave propagation. Technological developments in the 20th century enabled many other interesting applications of Huygens' principle. For example, in Equation (6), the wave field $p(\mathbf{x}', t)$ at $\mathbb{S}_0$ can be replaced by electric signals that are fed to a dense array of piezoelectric transducers which emit ultrasound. Equation (6) then describes the synthesized wave field emitted by the array into the half-space above $\mathbb{S}_0$. On the other hand, digitized measurements of an acoustic or seismic wave field $p(\mathbf{x}', t)$ at $\mathbb{S}_0$ can be fed to a computer and Equation (6) can be evaluated numerically to compute the wave field $p(\mathbf{x}, t)$ at any position $\mathbf{x}$ in the half-space above $\mathbb{S}_0$. The latter application is wave field extrapolation (Berkhout 1985). In practice, the convolution along the time coordinate is often replaced by a multiplication in the frequency domain (see Equation B9), but for clarity we keep our expressions in the time domain because this appeals better to the physics of Huygens' principle.

In Equation (6), $\mathbf{x}$ is assumed to be situated in the half-space above $\mathbb{S}_0$ whereas the source (or source distribution) of the wave field $p(\mathbf{x}', t)$ resides in the half-space below $\mathbb{S}_0$. For this situation, we speak of *forward* wave field extrapolation, since the direction of extrapolation (upward from $\mathbb{S}_0$ to $\mathbf{x}$ above $\mathbb{S}_0$) corresponds to the direction of the upgoing wave field $p(\mathbf{x}', t)$ at $\mathbb{S}_0$. Since this is the direction of the negative z-axis, we can indicate this with a superscript $-$ as follows:

$$p^-(\mathbf{x}, t) = -2 \int_{\mathbb{S}_0} G_\mathrm{d}(\mathbf{x}, \mathbf{x}', t) * p^-(\mathbf{x}', t)\mathrm{d}\mathbf{x}', \qquad (7)$$

for $\mathbf{x}$ above $\mathbb{S}_0$. Similarly, for forward extrapolation of a downgoing field, indicated with a superscript $+$, we can derive in a similar way

$$p^+(\mathbf{x}, t) = 2 \int_{\mathbb{S}_0} G_\mathrm{d}(\mathbf{x}, \mathbf{x}', t) * p^+(\mathbf{x}', t)\mathrm{d}\mathbf{x}', \qquad (8)$$

for $\mathbf{x}$ below $\mathbb{S}_0$ (here the source is assumed to be situated in the half-space above $\mathbb{S}_0$). Note that the dipole Green's function $G_\mathrm{d}(\mathbf{x}, \mathbf{x}', t)$ for $\mathbf{x}$ below $\mathbb{S}_0$ has a sign opposite to that for $\mathbf{x}$ above $\mathbb{S}_0$ (see Figure 2). This compensates for the different signs in front of the integrals in Equations (7) and (8).

2.2 | Inverse Wave Field Extrapolation Through a Homogeneous Medium

We start this section with discussing an intuitive modification of Huygens' principle for backpropagation. We consider again the acoustic pressure $p(\mathbf{x}, t)$ in a homogeneous lossless medium, in response to a source in the lower half-space (at $\mathbf{x}_S = (0, 1200)$ m), observed at $\mathbf{x}_n = (n\Delta x, z_0)$ at $\mathbb{S}_0$, with $n = -N, \ldots, -1, 0, 1, \ldots, N$ (with $N = 50$ and $\Delta x = 200$ m, hence $N\Delta x = 10{,}000$ m). In Equation (4), we replace the Green's function by the time-reversed Green's function $G_\mathrm{d}(\mathbf{x}, \mathbf{x}_n, -t)$ (i.e., the time-reversal of the dipole Green's function shown in Figure 2). Hence, we evaluate the expression

$$\langle p(\mathbf{x}, t) \rangle \propto 2 \sum_{n=-N}^{N} G_\mathrm{d}(\mathbf{x}, \mathbf{x}_n, -t) * p(\mathbf{x}_n, t), \qquad (9)$$

for $\mathbf{x}$ in the half-space below $\mathbb{S}_0$. The notation $\langle p(\mathbf{x}, t) \rangle$ means 'estimate of $p(\mathbf{x}, t)$'. Whereas, in Equation (4), the Green's function $G(\mathbf{x}, \mathbf{x}_n, t)$ forward propagates the field of the secondary sources $p(\mathbf{x}_n, t)$ into the half-space above $\mathbb{S}_0$, in Equation (9) the time-reversed Green's function $G_\mathrm{d}(\mathbf{x}, \mathbf{x}_n, -t)$ backpropagates the field of the secondary sources $p(\mathbf{x}_n, t)$ into the half-space below $\mathbb{S}_0$ (Schneider 1978). The result $\langle p(\mathbf{x}, t) \rangle$ for $t = 0.4$ s is shown in Figure 3a. This figure illustrates Huygens' superposition principle for backpropagation. The envelope of the superposed circular waves approximately forms a circular wave, resembling the wave emitted by the original point source at $\mathbf{x}_S$, observed above this point source at $t = 0.4$ s. Figure 3b shows $\langle p(\mathbf{x}, t) \rangle$ for $t = 0$ s. Here, a focus is formed at the position of the original point source. Since there is no sink at $\mathbf{x}_S$ to absorb the focused field, $\langle p(\mathbf{x}, t) \rangle$ does not vanish when we continue the backpropagation to negative times, as is shown in Figure 3c for $t = -0.4$ s. Next, we replace the summation in Equation (9) with an integration, according to

$$\langle p(\mathbf{x}, t) \rangle = 2 \int_{\mathbb{S}_0} G_\mathrm{d}(\mathbf{x}, \mathbf{x}', -t) * p(\mathbf{x}', t)\mathrm{d}\mathbf{x}' \qquad (10)$$

(but in the numerical implementation we actually evaluate Equation (9), with Δx reduced to $\Delta x = 10$ m, which is much smaller than the central wavelength of 100 m, and $N = 1000$, so that again $N\Delta x = 10{,}000$ m). Figure 3d shows a superposition of snapshots of $\langle p(\mathbf{x}, t) \rangle$ for $t = 0.4$ s, $t = 0$ s and $t = -0.4$ s. In the left-hand side of Equation (10), we still use the notation $\langle p(\mathbf{x}, t) \rangle$, indicating an approximation of $p(\mathbf{x}, t)$. The actual response to a point source at $\mathbf{x}_S$ is causal and consists of circular wave fronts around $\mathbf{x}_S$ at positive times only, whereas Figure 3d shows an incomplete response at positive time (a half-circle above $\mathbf{x}_S$), and a non-existing response at negative time (a half-circle below $\mathbf{x}_S$). In Appendix C, we review a step-by-step derivation of Equation (10). Ignoring evanescent waves, we arrive at Equation (C4), which has three terms on the right-hand side. The first of these terms is the integral in the right-hand side of Equation (10), explaining Figure 3d. The second term restores the missing half-circle below $\mathbf{x}_S$ at positive time and creates a half-circle above $\mathbf{x}_S$ at negative time. The third term suppresses the entire acausal response. Since the second and third terms require measurements at a boundary below the source and knowledge of the source at $\mathbf{x}_S$, they cannot be evaluated in most practical situations. By ignoring the second
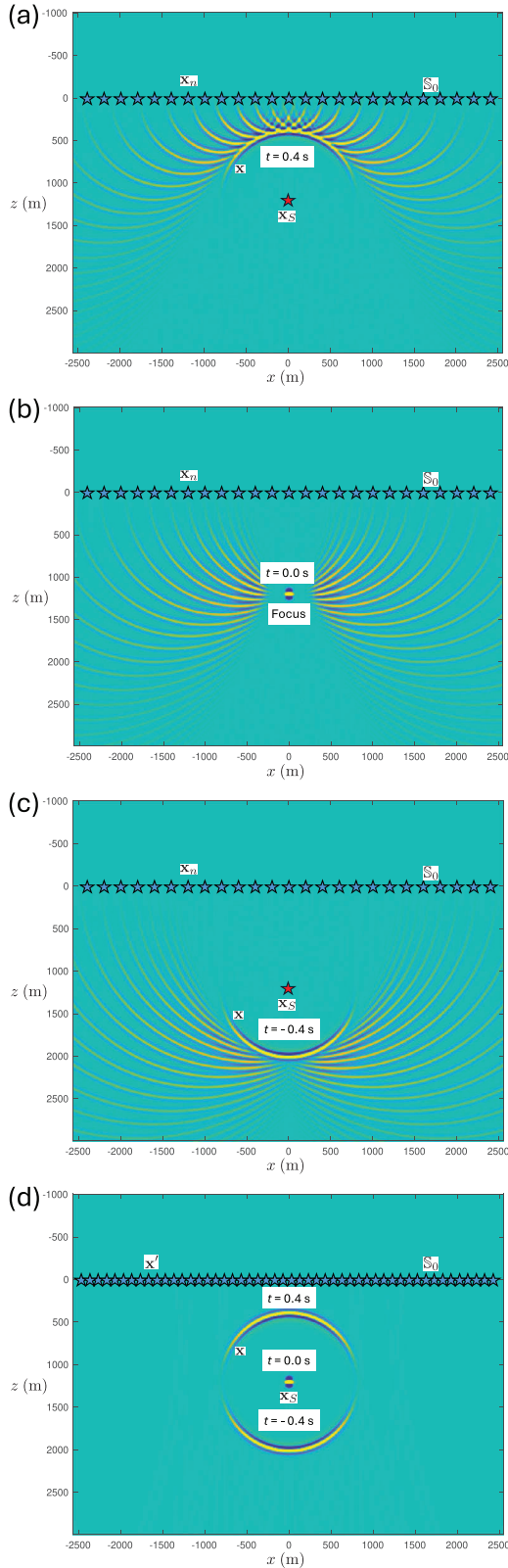
Figure 3 | (a)–(c) Illustration of Huygens' principle for backpropagation of acoustic waves in a homogeneous medium, according to Equation (9), with the time-reversal of the dipole Green's function of Figure 2. (d) As Figures (a)-(c), but here according to Equation (10).

and third terms in Equation (C4), we are left with Equation (10), with the limitations discussed above. For an inhomogeneous medium, the limitations are more severe as we will see in the next section.

Unlike Equation (6), which formalizes Huygens' explanation of the physics of wave propagation, Equation (10) with the time-reversed Green's function does not describe a physical situation. However, it can be used for numerical wave field extrapolation of an upgoing wave field $p(\mathbf{x}', t)$, measured at $\mathbb{S}_0$, to any position below $\mathbb{S}_0$ and above the source. Here, we speak of *inverse* wave field extrapolation, since the direction of extrapolation (downward from $\mathbb{S}_0$ to $\mathbf{x}$ below $\mathbb{S}_0$) is opposite to the direction of the upgoing wave field $p(\mathbf{x}', t)$ at $\mathbb{S}_0$. We indicate upgoing wave fields again with a superscript $-$ and replace Equation (10) by

$$p^-(\mathbf{x}, t) = 2 \int_{\mathbb{S}_0} G_{\mathrm{d}}(\mathbf{x}, \mathbf{x}', -t) * p^-(\mathbf{x}', t)\mathrm{d}\mathbf{x}', \qquad (11)$$

for $\mathbf{x}$ below $\mathbb{S}_0$. As long as $\mathbf{x}$ is above the source in the lower half-space, Equation (11) describes the complete upgoing wave field at $\mathbf{x}$; see Figure 3 (in this case, the only approximation is the neglection of evanescent waves). When the lower half-space is source-free, Equation (11) even holds for the entire lower half-space. Similarly, for inverse extrapolation of a downgoing wave field, we can derive in a similar way

$$p^+(\mathbf{x}, t) = -2 \int_{\mathbb{S}_0} G_{\mathrm{d}}(\mathbf{x}, \mathbf{x}', -t) * p^+(\mathbf{x}', t)\mathrm{d}\mathbf{x}', \qquad (12)$$

for $\mathbf{x}$ above $\mathbb{S}_0$. As long as $\mathbf{x}$ is below the source in the upper half-space, Equation (12) describes the complete downgoing wave field at $\mathbf{x}$. When the upper half-space is source-free, Equation (12) holds for the entire upper half-space.

Equations (11) and (12) are the basic expressions for inverse wave field extrapolation through a homogeneous lossless medium, as applied in acoustic and seismic imaging methods. They can be implemented in the space-time domain, as in Kirchhoff migration (Schneider 1978; Tygel et al. 2000) and reverse-time migration (Whitmore 1983; McMechan 1983), in the space-frequency domain, as in seismic inversion (Cohen et al. 1986) and seismic migration (Berkhout 1985), or in the wavenumber–frequency domain, as in migration with the phase-shift method (Gazdag 1978).

Another application of Equation (10) is obtained when we revert the time coordinate on the right-hand side, according to

$$2 \int_{\mathbb{S}_0} G_{\mathrm{d}}(\mathbf{x}, \mathbf{x}', t) * p(\mathbf{x}', -t)\mathrm{d}\mathbf{x}'. \qquad (13)$$

Note that $G_{\mathrm{d}}(\mathbf{x}, \mathbf{x}', t)$ is again the causal response to a dipole at $\mathbf{x}'$ on $\mathbb{S}_0$, similar to Equation (6). The expression of Equation (13) underlies the principle of time-reversed acoustics, as advocated by Fink (1992) and coworkers. In this situation, $p(\mathbf{x}', -t)$ represents the time reversal of measurements at $\mathbb{S}_0$, which are fed to a dense

array of piezoelectric transducers which emit ultrasound. This expression thus describes the synthesized wave field emitted by the array into the half-space below $\mathbb{S}_0$. If we interchange the labels for positive and negative times in Figure 3, this figure shows the synthesized wave field at $t = -0.4$ s converging to the position of the original source, the focused field at $t = 0$ s, and the field at $t = 0.4$ s diverging from the focus. Note that in this case the focused field acts as a downward radiating virtual source. A further discussion of time-reversed acoustics is beyond the scope of this paper.

2.3 | Inverse Wave Field Extrapolation Through an Inhomogeneous Medium

We discuss Huygens' principle for backpropagation through an inhomogeneous lossless medium. To show the essence, we consider for simplicity the horizontally layered medium of Figure 4, with interfaces (indicated by the yellow solid lines) at $z = 500$ m and $z = 1500$ m. The propagation velocity c is taken constant throughout at 2000 m/s. The mass density ρ in the half-spaces $z < 500$ m and $z > 1500$ m equals 1000 kg/m^3 and in the layer $500 < z < 1500$ m it equals 4000 kg/m^3. We place again a monopole source at $\mathbf{x}_S = (0, 1200)$ m (indicated by the red star), between the two interfaces. The source function is again a Ricker wavelet $s(t)$ with a central frequency of 20 Hz. We use a recursive 'layer-code' method (Kennett 1983) to model the response to this source. This response, $p(\mathbf{x}, t) = G(\mathbf{x}, \mathbf{x}_S, t) * s(t)$, is shown in Figure 4a–d for $t = 0.2$ s, $t = 0.4$ s, $t = 0.6$ s and $t = 0.8$ s (note that the amplitudes along the wave fronts are again tapered at large propagation angles). The interfaces at $z = 500$ m and $z = 1500$ m partially reflect and partially transmit the waves. Figure 4d shows the first multiply reflected wave.

For the same layered medium, the dipole Green's function $G_d(\mathbf{x}, \mathbf{x}', t)$, for a dipole at $\mathbf{x}'$ on $\mathbb{S}_0$, is shown in Figure 5. Snapshots of this Green's function for $t = 0.2$ s and $t = 0.4$ s are shown in Figure 5a, whereas Figure 5b shows a snapshot for $t = 1.4$ s, including the first multiply reflected event. Figure 5c is a cross section of $G_d(\mathbf{x}, \mathbf{x}', t)$ along a vertical line through the dipole source, as a function of depth z and time t. The vertical dashed lines in this figure at $t = 0.2$ s, $t = 0.4$ s and $t = 1.4$ s correspond to the vertical dashed lines in the snapshots in Figure 5a,b. The vertical solid line in Figure 5c at $t = 0$ s indicates the causality condition, which states that $G_d(\mathbf{x}, \mathbf{x}', t)$ is non-zero only after the source at $t = 0$ (hence, right of this line). Figure 5d is a ray diagram of this dipole Green's function.

We use the time-reversal of the dipole Green's function of Figure 5 to backpropagate the acoustic pressure wave field of Figure 4 from $\mathbb{S}_0$ to any point $\mathbf{x}$ below $\mathbb{S}_0$. First, we use the discretized form of Huygens' principle, as formulated by Equation (9), with $\mathbf{x}_n = (n\Delta x, z_0)$, $\Delta x = 200$ m and $N = 50$. The results $\langle p(\mathbf{x}, t) \rangle$ for $t = 0.8$ s and $t = 0.4$ s are shown in Figure 6a and 6b. Compare these figures with Figure 4d and 4b, which show the desired field $p(\mathbf{x}, t)$ at the same time instants. It appears that the envelopes of the superposed waves in Figure 6a,b resemble parts of the desired field, but significant parts are missing (in particular, the downgoing field in the lower half-space), the amplitudes of the reflected waves are too low, and circular ghost events appear in the lower half-space. Figure 6c shows $\langle p(\mathbf{x}, t) \rangle$ for
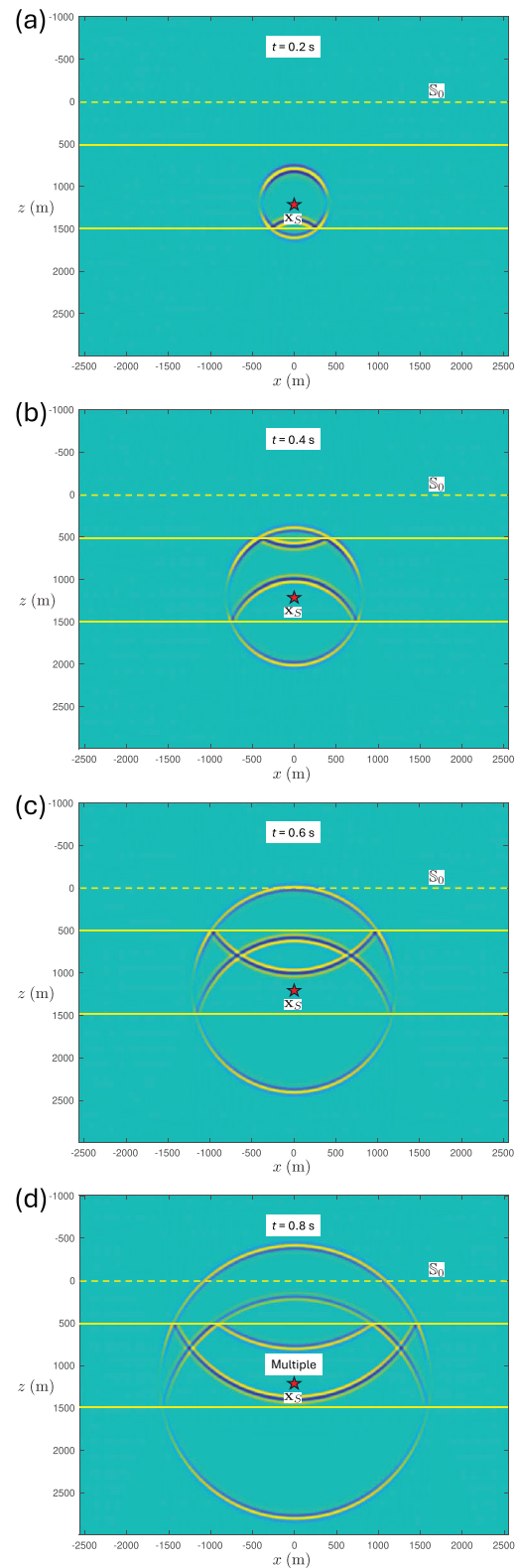
Figure 4 | Wave field $p(\mathbf{x}, t) = G(\mathbf{x}, \mathbf{x}_S, t) * s(t)$ in a layered medium, for a monopole at $\mathbf{x}_S$.

$t = 0$ s. Apart from the focus on the position of the original point source, a ghost focus is formed below the second interface. Figure 6d shows $\langle p(\mathbf{x}, t) \rangle$ for $t = -0.4$ s. Clearly, $\langle p(\mathbf{x}, t) \rangle$ does not vanish for negative times. The situation is more complex than in Figure 3, which is the result of applying Equation (9) in a homogeneous medium. In particular, reflected waves are
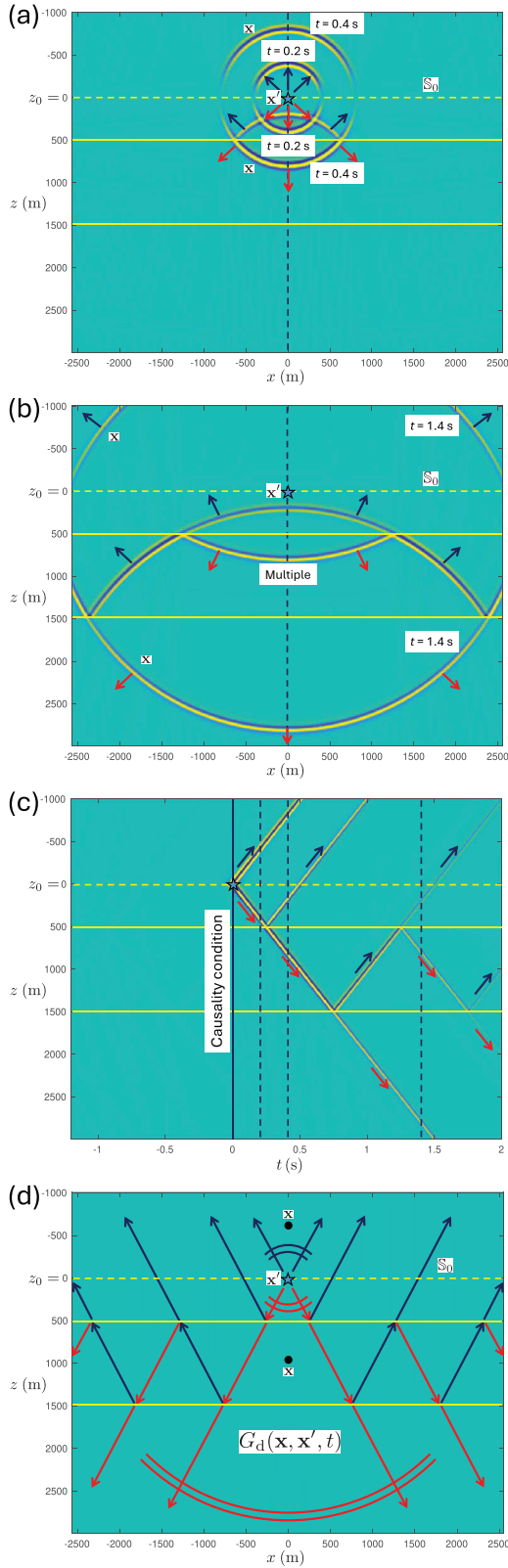
Figure 5 | (a) and (b) Dipole Green's function $G_d(\mathbf{x}, \mathbf{x}', t)$ (convolved with a Ricker wavelet) in a layered medium, for a dipole at $\mathbf{x}'$ on $\mathbb{S}_0$ at depth z_0. (c) Cross section at $x = x' = 0$. (d) Ray diagram. Red and blue arrows represent downgoing and upgoing waves, respectively. The arcs represent some of the wave fronts at $t = 0.2$ s and $t = 1.4$ s.

not correctly backpropagated by the time-reversed dipole Green's function of the layered medium, despite the fact that primary and multiply reflected waves are included in this Green's function (see Figure 5).

Next, we use the integral form of Huygens' principle, as formulated by Equation (10), which we extend with a second integral over a boundary $\mathbb{S}_1$ (at $z_1 = 3000$ m) below the source, hence

$$\langle p(\mathbf{x}, t)\rangle = 2 \int_{\mathbb{S}_0} G_d(\mathbf{x}, \mathbf{x}', -t) * p(\mathbf{x}', t)\mathrm{d}\mathbf{x}'$$

$$-2 \int_{\mathbb{S}_1} G_d(\mathbf{x}, \mathbf{x}', -t) * p(\mathbf{x}', t)\mathrm{d}\mathbf{x}', \qquad (14)$$

for $\mathbf{x}$ between $\mathbb{S}_0$ and $\mathbb{S}_1$. The results $\langle p(\mathbf{x}, t)\rangle$ for $t = 0.8$ s and $t = 0.4$ s are shown in Figure 7a,b. These results accurately resemble the desired field $p(\mathbf{x}, t)$, shown in Figure 4d and 4b, respectively, including the internal multiply reflected waves. Figure 7c, which shows $\langle p(\mathbf{x}, t)\rangle$ for $t = 0$ s, contains a single focus at the position of the original point source. Finally, Figure 7d shows $\langle p(\mathbf{x}, t)\rangle$ for $t = -0.4$ s, which again appears to be non-zero. Comparing Equation (14) with Equation (C4), we find that $\langle p(\mathbf{x}, t)\rangle$ consists of two contributions, according to

$$\langle p(\mathbf{x}, t)\rangle = p(\mathbf{x}, t) + G(\mathbf{x}, \mathbf{x}_S, -t) * s(t). \qquad (15)$$

The second term in this expression explains the contribution at negative time in Figure 7d.

In most practical situations, measurements are available only at a single boundary, say $\mathbb{S}_0$, meaning that the second integral in Equation (14) cannot be evaluated. Hence, we are left with the integral along $\mathbb{S}_0$, as formulated by Equation (10), with $G_d(\mathbf{x}, \mathbf{x}', -t)$ defined in the inhomogeneous medium. Similar to a homogeneous medium, we can reformulate this again into Equation (11), which then describes approximate inverse extrapolation of upgoing waves $p^-(\mathbf{x}', t)$ from $\mathbb{S}_0$ through an inhomogeneous medium, to $\mathbf{x}$ below $\mathbb{S}_0$ and above the source in the lower half-space. As we have seen above, this approximation does not properly handle multiply reflected waves, so it only accounts for primary waves. Moreover, even for these primary waves, amplitude errors occur, which are proportional to amplitudes of multiply reflected waves (see Wapenaar et al. 1989 for a detailed analysis). Despite these approximations, Equation (11), with the dipole Green's function defined in the inhomogeneous medium, forms the basis for many acoustic and seismic imaging schemes, including reverse time migration, time-reversed acoustics, etc. The approximations are acceptable as long as the contrasts in the medium are sufficiently small so that internal multiply reflected waves can be ignored. For situations in which internal multiply reflected waves cannot be ignored, other approaches are needed. One of these approaches is the replacement of the dipole Green's functions by focusing functions. This modification of Huygens' principle is the subject of the next section.
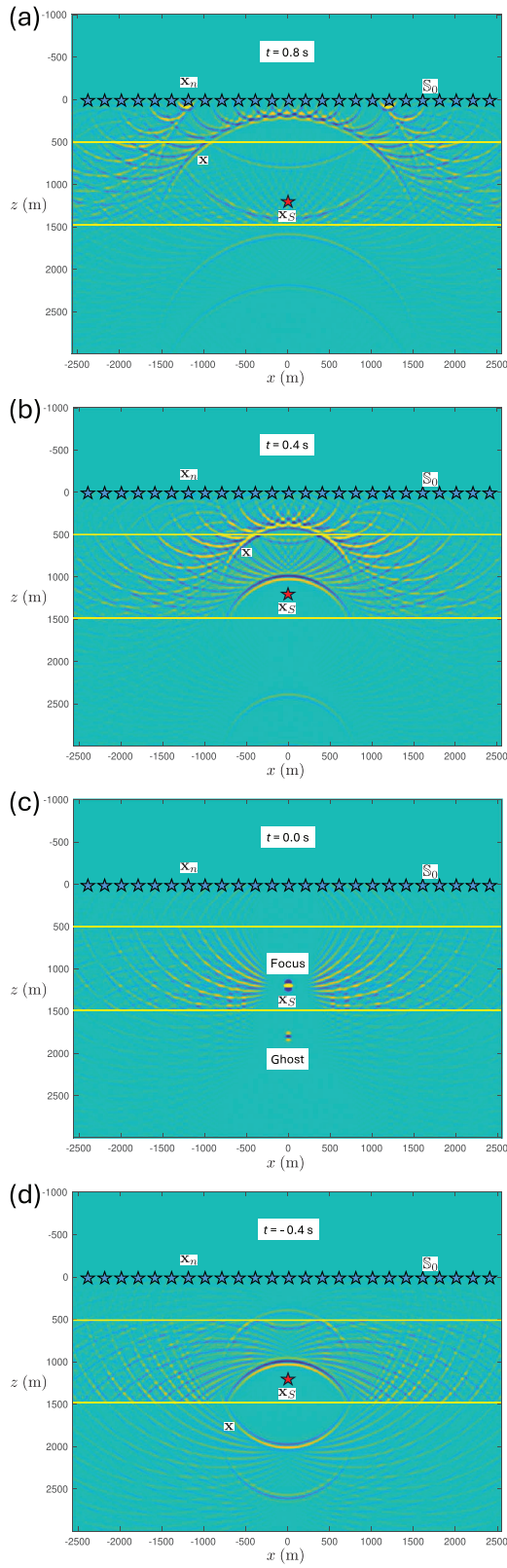
Figure 6 | Illustration of Huygens' principle for backpropagation of acoustic waves in a layered medium (Equation (9), with the time-reversal of the dipole Green's function of Figure 5).
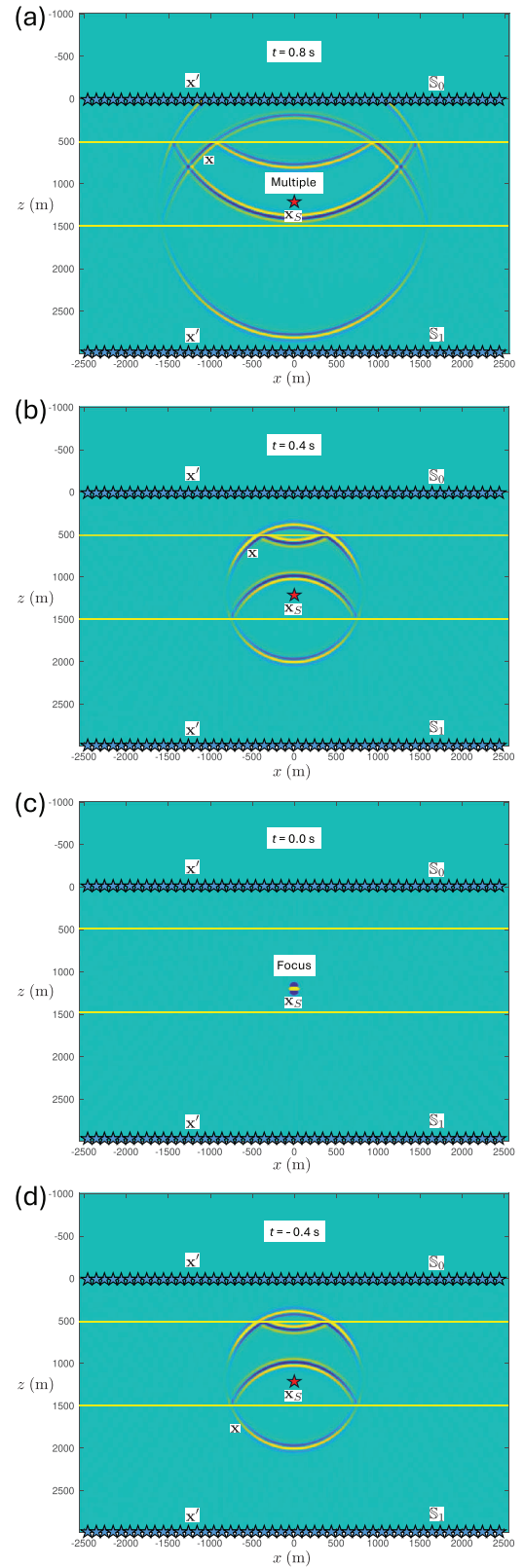
Figure 7 | Illustration of Huygens' principle for backpropagation of acoustic waves in a layered medium from two enclosing boundaries (Equation 14).

We conclude this section by deriving a representation for the homogeneous Green's function from Equations (14) and (15). Using Equation (2) for the first term on the right-hand side of Equation (15), we observe that this equation can be written as $\langle p(\mathbf{x}, t) \rangle = G_{\mathrm{h}}(\mathbf{x}, \mathbf{x}_S, t) * s(t)$, where $G_{\mathrm{h}}(\mathbf{x}, \mathbf{x}_S, t)$ is the homogeneous Green's function, defined as

$$G_{\mathrm{h}}(\mathbf{x}, \mathbf{x}_S, t) = G(\mathbf{x}, \mathbf{x}_S, t) + G(\mathbf{x}, \mathbf{x}_S, -t); \qquad (16)$$

see Appendix A2 (here, 'homogeneous' refers to the fact that the wave equation for G_{h} has no source term; hence, it is a homogeneous differential equation). Next, using this in the left-hand side of Equation (14) and using Equation (2) for $p(\mathbf{x}', t)$ in the right-hand side of Equation (14), we obtain (after removing the convolution with $s(t)$ on both sides) the following representation for the homogeneous Green's function in an inhomogeneous lossless medium:

$$G_{\mathrm{h}}(\mathbf{x}, \mathbf{x}_S, t) = 2 \int_{\mathbb{S}_0} G_{\mathrm{d}}(\mathbf{x}, \mathbf{x}', -t) * G(\mathbf{x}', \mathbf{x}_S, t) \mathrm{d}\mathbf{x}'$$
$$- 2 \int_{\mathbb{S}_1} G_{\mathrm{d}}(\mathbf{x}, \mathbf{x}', -t) * G(\mathbf{x}', \mathbf{x}_S, t) \mathrm{d}\mathbf{x}' \qquad (17)$$

(Porter 1970; Oristaglio 1989). This representation forms the basis for holographic imaging and inverse scattering methods. Moreover, if we use the source–receiver reciprocity relation $G(\mathbf{x}', \mathbf{x}_S, t) = G(\mathbf{x}_S, \mathbf{x}', t)$, then the integrands on the right-hand side describe the cross-correlation of responses at receivers at $\mathbf{x}_S$ and $\mathbf{x}$ (both located between $\mathbb{S}_0$ and $\mathbb{S}_1$), due to sources at $\mathbf{x}'$ at the boundaries $\mathbb{S}_0$ and $\mathbb{S}_1$ (Wapenaar and Fokkema 2006). In this form, Equation (17) is the theoretical basis for Green's function retrieval, also known as seismic interferometry (Weaver and Lobkis 2001; Campillo and Paul 2003; Schuster et al. 2004; Snieder 2004; Roux et al. 2004; Sabra et al. 2007; Draganov et al. 2009). Again, in many practical situations (for holographic imaging, interferometry, etc.), receivers or sources are available only at a single boundary. An alternative representation of the homogeneous Green's function, in terms of integrals over a single boundary, follows from the modified version of Huygens' principle in the next section.

3 | Modified Huygens' Principle, Using Focusing Functions

3.1 | Introducing the Focusing Function

Huygens' principle, formalized by Kirchhoff, Rayleigh and others, accurately explains the physics of wave propagation. As we have seen, it can also be used for forward extrapolation of a wave field measured on a plane $\mathbb{S}_0$ into a source-free half-space. This is formulated by Equation (6) and illustrated for a homogeneous upper half-space in Figure 1. When the upper half-space is inhomogeneous, Equation (6) still holds when the dipole Green's function is replaced by that of the inhomogeneous upper half-space (and the wave field at $\mathbb{S}_0$ by its upgoing part). Hence, for these situations, there is no need to modify the mathematical formulation of Huygens' principle.

For inverse wave field extrapolation (i.e., extrapolation of a wave field measured on a plane $\mathbb{S}_0$ into the half-space containing the source(s) of this wave field), the dipole Green's function is commonly replaced by its time-reversed version (see Equation 10). This is illustrated for a homogeneous lower half-space in Figure 3 and for an inhomogeneous lower half-space (using the time-reversed dipole Green's function of this inhomogeneous half-space) in Figure 6. In the latter case, inverse wave field extrapolation yields reasonable results for the primary waves but it breaks down for multiply reflected waves, even though these are included in the Green's functions.

Huygens' principle was meant to explain the physics of wave propagation, so the fact that it has limitations for inverse wave field extrapolation is not a shortcoming of this principle in itself. Nevertheless, it is worthwhile to modify Huygens' principle for inverse wave field extrapolation, in such a way that it accounts for multiply reflected waves. To address this, in this section, we replace the dipole Green's functions by focusing functions and, hence, the dipole sources by focal points. In previous work on the Marchenko method, we introduced two types of focusing functions: f_1, which has a focal point inside the inhomogeneous medium, and f_2, with its focal point at the boundary between the inhomogeneous lower half-space and the homogeneous upper half-space (Wapenaar et al. 2014). Since the dipole Green's functions in Huygens' principle have their sources at the boundary $\mathbb{S}_0$, we choose for focusing functions with their focal points at $\mathbb{S}_0$. Hence, the focusing function F we discuss below is akin to the focusing function f_2. However, it is normalized in a different way. Moreover, whereas f_2 is defined in a truncated version of the actual medium, the focusing function F is defined in the actual medium and it is not decomposed into downgoing and upgoing components inside the medium. Before we discuss this focusing function in an inhomogeneous medium, we start with discussing the focusing function F in a homogeneous medium.

3.2 | Focusing Function in a Homogeneous Medium

We define the focusing function $F(\mathbf{x}, \mathbf{x}', t)$ for a homogeneous lossless medium as an upward propagating wave field, of which the wave fronts are half-spheres (in three dimensions) or half-circles (in two dimensions) centred at $\mathbf{x}'$ on $\mathbb{S}_0$ (at depth z_0) (see Figure 8a for the 2D situation). At negative times, the focusing function propagates (as a function of $\mathbf{x}$ and t) upward through the lower half-space towards $\mathbb{S}_0$, at $t = 0$ it focuses at $\mathbf{x} = \mathbf{x}'$ on $\mathbb{S}_0$, and at positive times it propagates upward through the upper half-space away from $\mathbb{S}_0$. The time-reversed focusing function $F(\mathbf{x}, \mathbf{x}', -t)$, illustrated in Figure 8b for the 2D situation, propagates at negative times downward through the upper half-space towards $\mathbb{S}_0$, at $t = 0$ it focuses at $\mathbf{x} = \mathbf{x}'$ on $\mathbb{S}_0$, and at positive times it propagates downward through the lower half-space away from $\mathbb{S}_0$.

In the lower half-space, we relate the upward propagating focusing function of Figure 8a to the time-reversal of the dipole Green's function of Figure 2 via

$$F(\mathbf{x}, \mathbf{x}', t) = 2 G_{\mathrm{d}}(\mathbf{x}, \mathbf{x}', -t), \qquad (18)$$
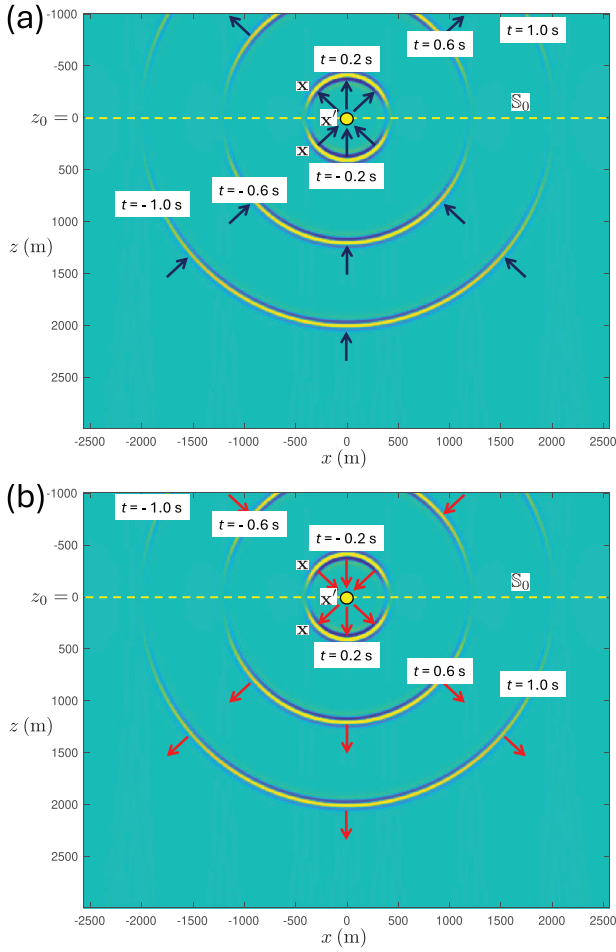
Figure 8 | (a) Focusing function $F(\mathbf{x}, \mathbf{x}', t)$ (convolved with a Ricker wavelet to get a nicer display) and (b) its time-reversed version $F(\mathbf{x}, \mathbf{x}', -t)$ in a homogeneous medium, for a focal point at $\mathbf{x}'$ on $\mathbb{S}_0$ at depth z_0. In the modified version of Huygens' principle for a homogeneous medium (Equations 21 and 22), these focusing functions replace the dipole Green's function of Figure 2.

for $\mathbf{x}$ below $\mathbb{S}_0$. In the upper half-space, we relate it to the dipole Green's function via

$$F(\mathbf{x}, \mathbf{x}', t) = -2G_{\mathrm{d}}(\mathbf{x}, \mathbf{x}', t), \qquad (19)$$

for $\mathbf{x}$ above $\mathbb{S}_0$. For $\mathbf{x}$ at $\mathbb{S}_0$ (hence, for $z = z' = z_0$), the focusing condition reads

$$F(\mathbf{x}, \mathbf{x}', t)|_{z=z'} = \delta(\mathbf{x}_{\mathrm{H}} - \mathbf{x}'_{\mathrm{H}})\delta(t), \qquad (20)$$

where $\mathbf{x}_{\mathrm{H}}$ and $\mathbf{x}'_{\mathrm{H}}$ denote the horizontal components of $\mathbf{x}$ and $\mathbf{x}'$, respectively, hence $\mathbf{x}_{\mathrm{H}} = (x, y)$ and $\mathbf{x}'_{\mathrm{H}} = (x', y')$ (in three dimensions) or $\mathbf{x}_{\mathrm{H}} = x$ and $\mathbf{x}'_{\mathrm{H}} = x'$ (in two dimensions). In theory, evanescent waves can be included in the focusing function (Dukalski et al. 2022; Wapenaar et al. 2023), but to avoid instability they are usually suppressed. This implies that the delta functions in the right-hand side of Equation (20) should be interpreted as band-limited delta functions. Note that, whereas the Green's function $G_{\mathrm{d}}(\mathbf{x}, \mathbf{x}', t)$ is the response to a dipole source at $\mathbf{x}'$ on $\mathbb{S}_0$, the focusing function $F(\mathbf{x}, \mathbf{x}', t)$ obeys a source-free wave

equation (the right-hand side of Equation (20) formulates a focusing condition, not a source; see Appendix D for details).

Substituting Equation (19) into Equation (7) for forward extrapolation of upgoing waves to $\mathbf{x}$ above $\mathbb{S}_0$, or substituting Equation (18) into Equation (11) for inverse extrapolation of upgoing waves to $\mathbf{x}$ below $\mathbb{S}_0$, we obtain in both cases

$$p^-(\mathbf{x}, t) = \int_{\mathbb{S}_0} F(\mathbf{x}, \mathbf{x}', t) * p^-(\mathbf{x}', t)\mathrm{d}\mathbf{x}'. \qquad (21)$$

Hence, this expression holds for $\mathbf{x}$ in the upper as well as the lower half-space as long as $\mathbf{x}$ is above the source in the lower half-space. Similarly, substituting Equation (18) into Equation (8) for forward extrapolation of downgoing waves to $\mathbf{x}$ below $\mathbb{S}_0$, or substituting Equation (19) into Equation (12) for inverse extrapolation of downgoing waves to $\mathbf{x}$ above $\mathbb{S}_0$, we obtain in both cases

$$p^+(\mathbf{x}, t) = \int_{\mathbb{S}_0} F(\mathbf{x}, \mathbf{x}', -t) * p^+(\mathbf{x}', t)\mathrm{d}\mathbf{x}'. \qquad (22)$$

Hence, this expression also holds for $\mathbf{x}$ in the upper and lower half-space as long as $\mathbf{x}$ is below the source in the upper half-space. In the absence of sources, Equations (21) and (22) hold throughout space.

By introducing the focusing function and its time-reversal, we achieved that the four equations for forward and inverse extrapolation of upgoing and downgoing waves through a homogeneous medium (Equations 7, 8, 11 and 12) are now captured by the two Equations (21) and (22). These equations formulate modified versions of Huygens' principle for a homogeneous medium. Figures 1 and 3 can be seen as examples of Equation (21) for $\mathbf{x}$ above and below $\mathbb{S}_0$, respectively. For a homogeneous medium, there are no further advantages of using the focusing functions instead of the dipole Green's functions. This changes considerably for an inhomogeneous medium.

3.3 | Focusing Function in an Inhomogeneous Medium

We consider a medium which is inhomogeneous below the boundary $\mathbb{S}_0$ (at depth z_0), with propagation velocity $c(\mathbf{x})$ and mass density $\rho(\mathbf{x})$. At and above this boundary, we assume that the medium is homogeneous, with propagation velocity c_0 and mass density ρ_0. For this configuration, we define the focusing function $F(\mathbf{x}, \mathbf{x}', t)$, with $\mathbf{x}'$ again denoting a focal point at $\mathbb{S}_0$ (hence, $z' = z_0$). Throughout space, $F(\mathbf{x}, \mathbf{x}', t)$ obeys the source-free acoustic wave equation, with the condition that at $\mathbb{S}_0$ it obeys the focusing condition, formulated by Equation (20), and that at and above $\mathbb{S}_0$ it propagates upward. Hence, at and above $\mathbb{S}_0$ this focusing function is the same as that for a homogeneous medium, discussed in the previous section; below $\mathbb{S}_0$, it is of course different. Assuming the medium is lossless throughout space, the time-reversed focusing function $F(\mathbf{x}, \mathbf{x}', -t)$ obeys the same source-free wave equation as $F(\mathbf{x}, \mathbf{x}', t)$. At and above $\mathbb{S}_0$, this time-reversed focusing function propagates downward.

We illustrate $F(\mathbf{x}, \mathbf{x}', t)$ for the same layered medium as used for previous examples. Figure 9a–d shows snapshots at times
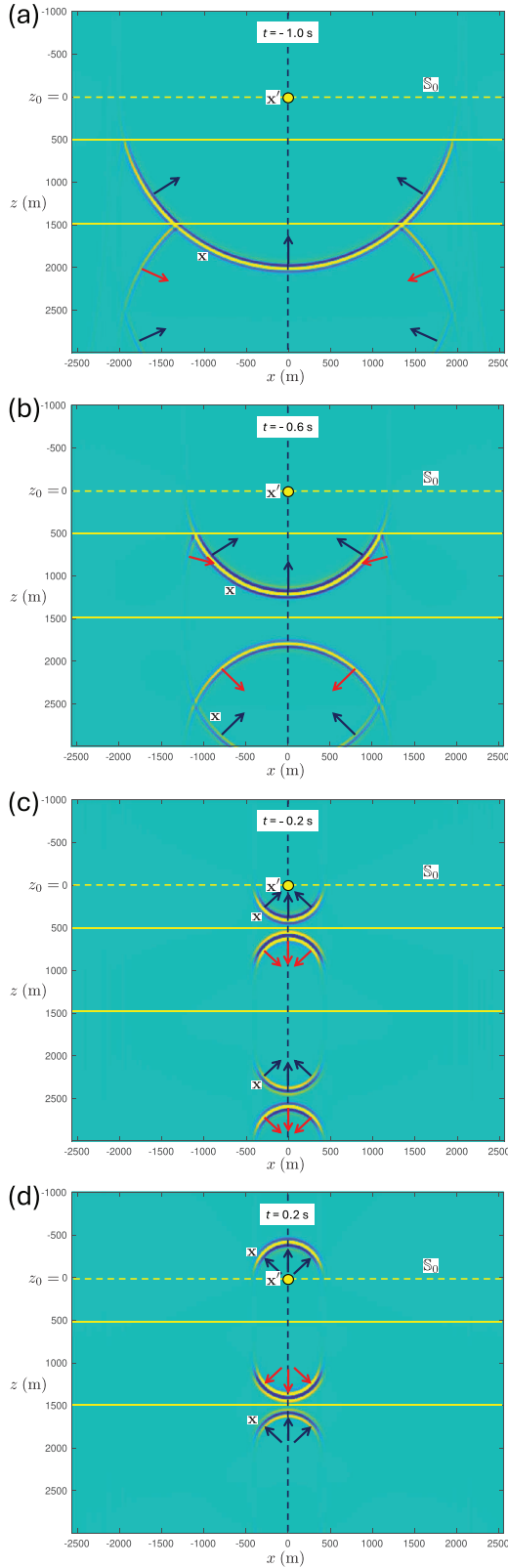
Figure 9 | Focusing function $F(\mathbf{x}, \mathbf{x}', t)$ (convolved with a Ricker wavelet) in a layered medium, for a focal point at $\mathbf{x}'$ on $\mathbb{S}_0$ at depth z_0. In the modified version of Huygens' principle for an inhomogeneous medium (Equation 23), this focusing function and its time-reversed version replace the dipole Green's function of Figure 5.

$t = -1.0$ s, $t = -0.6$ s, $t = -0.2$ s and $t = 0.2$ s, respectively. Figure 10a,b shows cross sections of $F(\mathbf{x}, \mathbf{x}', t)$, and of its time-reversed version $F(\mathbf{x}, \mathbf{x}', -t)$, along a vertical line through the focal point, as a function of depth z and time t. The vertical dashed lines in Figure 10a at $t = -1.0$ s, $t = -0.6$ s, $t = -0.2$ s and $t = 0.2$ s correspond to the vertical dashed lines in the snapshots in Figure 9a–d. Figure 10c,d shows ray diagrams of $F(\mathbf{x}, \mathbf{x}', t)$ and $F(\mathbf{x}, \mathbf{x}', -t)$. From these figures, we observe that the focusing function $F(\mathbf{x}, \mathbf{x}', t)$ starts with upgoing waves in the half-space below the deepest interface, which are tuned in such a way that, after interaction at the interfaces, a single upgoing wave converges to the focal point (Figures 9c and 10c), focuses at $\mathbf{x} = \mathbf{x}'$ and $t = 0$ and continues as a single upgoing wave, diverging from the focal point (Figures 9d and 10c).

Note the different character of the focusing function $F(\mathbf{x}, \mathbf{x}', t)$ in Figures 9 and 10 in comparison with the dipole Green's function $G_\mathrm{d}(\mathbf{x}, \mathbf{x}', t)$ in Figure 5. Whereas the dipole Green's function obeys a causality condition related to the source at $t = 0$, indicated by the vertical solid line in Figure 5c, the focusing function obeys a focusing condition at z_0, indicated by the horizontal solid lines in Figure 10a,b. Conversely, the focusing function is not causal (it exists at negative and positive times; see Figure 10a), whereas the dipole Green's function does not focus at z_0 (it contains multiple upgoing events at z_0; see Figure 5c,d).

3.4 | Modified Huygens' Principle for an Inhomogeneous Medium

We now discuss how the focusing functions $F(\mathbf{x}, \mathbf{x}', t)$ and $F(\mathbf{x}, \mathbf{x}', -t)$ can replace the dipole Green's functions $G_\mathrm{d}(\mathbf{x}, \mathbf{x}', t)$ and $G_\mathrm{d}(\mathbf{x}, \mathbf{x}', -t)$ in Huygens' principle for an inhomogeneous medium. Recall that we assume that the medium at and above the boundary $\mathbb{S}_0$ is homogeneous, with propagation velocity c_0 and mass density ρ_0. This means that in the upper half-space we can handle downgoing and upgoing waves independently of each other. On the other hand, the medium below $\mathbb{S}_0$ is inhomogeneous with propagation velocity $c(\mathbf{x})$ and mass density $\rho(\mathbf{x})$. Although in inhomogeneous media, decomposition into downgoing and upgoing waves is often possible locally, in the following analysis we will not make use of this, so in the lower half-space we will consider the total wave field. For the moment, we will assume that the entire medium (at, above and below $\mathbb{S}_0$) is source-free for the wave field $p(\mathbf{x}, t)$. Hence, $p(\mathbf{x}, t)$ obeys the wave equation $\mathcal{L} p = 0$ (with $\mathcal{L}$ defined in Equation (A2)) in the entire medium. The focusing functions $F(\mathbf{x}, \mathbf{x}', t)$ and $F(\mathbf{x}, \mathbf{x}', -t)$ obey the same source-free wave equation.

In the previous section, we remarked that at and above $\mathbb{S}_0$, the focusing function $F(\mathbf{x}, \mathbf{x}', t)$ is the same as that for a homogeneous medium. Hence, Equations (21) and (22), which were derived for $\mathbf{x}$ in the upper and lower half-space in a homogeneous medium, still hold for $\mathbf{x}$ in the homogeneous half-space above $\mathbb{S}_0$, even when the medium below $\mathbb{S}_0$ is inhomogeneous. Defining $p(\mathbf{x}, t) = p^-(\mathbf{x}, t) + p^+(\mathbf{x}, t)$ for $\mathbf{x}$ at and above $\mathbb{S}_0$, we obtain from Equations (21) and (22)

$$p(\mathbf{x}, t) = \int_{\mathbb{S}_0} F(\mathbf{x}, \mathbf{x}', t) * p^-(\mathbf{x}', t) \mathrm{d}\mathbf{x}'$$
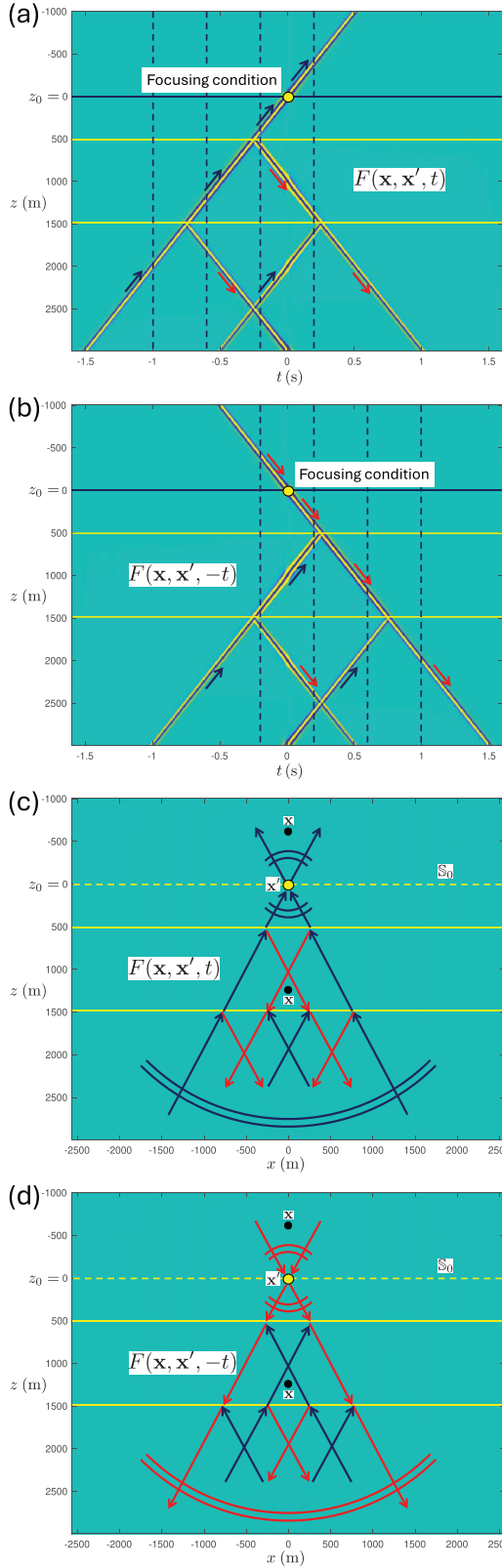
Figure 10 | (a) and (b) Cross sections at $x = x' = 0$ and (c) and (d) ray diagrams of the focusing function $F(\mathbf{x}, \mathbf{x}', t)$ in Figure 9 and of its time-reversed version $F(\mathbf{x}, \mathbf{x}', -t)$. Red and blue arrows represent downgoing and upgoing waves, respectively. The arcs represent some of the wave fronts at $t = \mp 1.4$ s and $t = \mp 0.2$ s.

$$+ \int_{\mathbb{S}_0} F(\mathbf{x}, \mathbf{x}', -t) * p^+(\mathbf{x}', t) \mathrm{d}\mathbf{x}', \qquad (23)$$

for $\mathbf{x}$ at and above $\mathbb{S}_0$. The focusing functions $F(\mathbf{x}, \mathbf{x}', t)$ and $F(\mathbf{x}, \mathbf{x}', -t)$ are mutually independent solutions of the same source-free wave equation as that for $p(\mathbf{x}, t)$. Hence, from a mathematical viewpoint, Equation (23) expresses $p(\mathbf{x}, t)$ as a superposition of these independent solutions, with $p^-(\mathbf{x}', t)$ and $p^+(\mathbf{x}', t)$ being their (convolutional) coefficients. Although we derived this equation from Equations (21) and (22) for $\mathbf{x}$ at and above $\mathbb{S}_0$, the quantities $p(\mathbf{x}, t)$, $F(\mathbf{x}, \mathbf{x}', t)$ and $F(\mathbf{x}, \mathbf{x}', -t)$ all obey the same source-free wave equation for all $\mathbf{x}$ (at, above and below $\mathbb{S}_0$). Hence, if we write $p(\mathbf{x}, t)$ for $\mathbf{x}$ below $\mathbb{S}_0$ as a superposition of $F(\mathbf{x}, \mathbf{x}', t)$ and $F(\mathbf{x}, \mathbf{x}', -t)$, the coefficients must be the same as for $\mathbf{x}$ at and above $\mathbb{S}_0$. In other words, Equation (23) holds for all $\mathbf{x}$ throughout space. When there are sources for the wave field $p(\mathbf{x}, t)$ in the upper half-space, then Equation (23) holds for all $\mathbf{x}$ below the shallowest source (following the same reasoning as for the homogeneous medium). A more formal derivation of Equation (23) for all $\mathbf{x}$ below the shallowest source is presented in Appendix D. From this derivation, it also follows that evanescent waves are neglected at $\mathbb{S}_0$. This does not mean that evanescent waves are neglected altogether. Waves that are propagating at $\mathbb{S}_0$ may become evanescent in high-velocity layers, and Equation (23) accounts for such evanescent waves (Wapenaar et al. 2021).

Equation (23) formulates the modified Huygens' principle for an inhomogeneous medium. The two terms on the right-hand side are illustrated with ray diagrams in Figure 11 for $\mathbf{x}$ below $\mathbb{S}_0$. First, consider Figure 11b. A downgoing wave field $p^+(\mathbf{x}', t)$ is incident from above to the inhomogeneous lower half-space. For each $\mathbf{x}'$ on $\mathbb{S}_0$, it is convolved with the time-reversed focusing function $F(\mathbf{x}, \mathbf{x}', -t)$. The integral over all $\mathbf{x}'$ on $\mathbb{S}_0$, as formulated in the second term on the right-hand side of Equation (23), extrapolates the field $p^+(\mathbf{x}', t)$ from $\mathbb{S}_0$ into the lower half-space. Since the focusing function implicitly consists of a superposition of downgoing and upgoing waves in the lower half-space (the red and blue rays in Figure 11b), the result of this integral is *not* the forward extrapolated downgoing field $p^+(\mathbf{x}, t)$ in the lower half-space (unlike in the homogeneous medium situation, as formulated by Equation 22). Next, we consider Figure 11a. Here, the upgoing field $p^-(\mathbf{x}', t)$ is convolved with the focusing function $F(\mathbf{x}, \mathbf{x}', t)$ for all $\mathbf{x}'$ on $\mathbb{S}_0$. The integral over all $\mathbf{x}'$ on $\mathbb{S}_0$ (the first term on the right-hand side of Equation (23)) extrapolates the field $p^-(\mathbf{x}', t)$ from $\mathbb{S}_0$ into the lower half-space. For similar reasons as above, this is *not* the inverse extrapolated upgoing field $p^-(\mathbf{x}, t)$ in the lower half-space. However, the superposition of the two integrals, as formulated by Equation (23), yields the total wave field $p(\mathbf{x}, t)$ in the lower half-space, including all internal multiply reflected waves. In comparison with Equation (14), where the two integrals are taken over two different boundaries, in Equation (23) the two integrals are taken over one and the same boundary. Hence, this makes Equation (23) very useful for practical situations in which a medium is often accessible from one side only, such as in the seismic reflection method. The focusing function can be retrieved from the reflection response, acquired at the same boundary, using the Marchenko method for
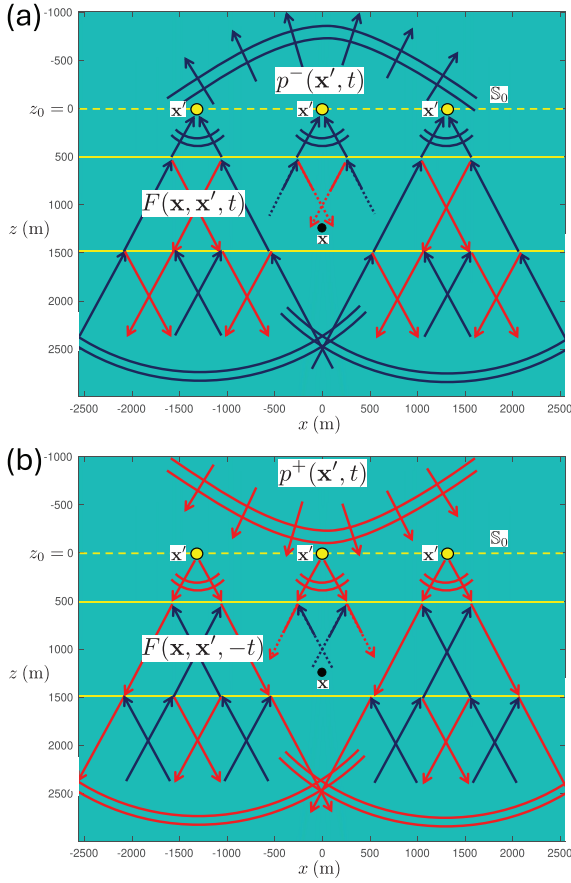
Figure 11 | Ray diagrams of the modified Huygens' principle, as formulated by Equation (23), with the focusing functions of Figure 10. (a) The first and (b) the second term in Equation (23).

1D, 2D or 3D inhomogeneous media (Broggini and Snieder 2012; Wapenaar et al. 2014; Slob et al. 2014; Van der Neut et al. 2015; Meles et al. 2015). In most papers on the Marchenko method, it is assumed that the wave field and focusing functions inside the medium can be decomposed into downgoing and upgoing components. This decomposition is avoided in Equation (23), which opens the way to handle refracted and evanescent waves (Wapenaar et al. 2021; Diekmann and Vasconcelos 2021). A further discussion of the Marchenko method is beyond the scope of this paper. In the next sections, we indicate applications of Equation (23), assuming the focusing function is known (either from numerical modelling or from applying the Marchenko method to the reflection response).

3.5 | Simultaneous Forward and Inverse Wave Field Extrapolation Through an Inhomogeneous Medium

Since Equation (23) yields the total wave field in the inhomogeneous half-space below $\mathbb{S}_0$ from downgoing and upgoing waves at $\mathbb{S}_0$, we can interpret it as an expression for simultaneous forward and inverse wave field extrapolation. We illustrate this for the situation of reflection measurements at the boundary $\mathbb{S}_0$. We define the reflection response $R(\mathbf{x}', \mathbf{x}'', t)$ of the inhomogeneous

lower half-space via the relation

$$p^-(\mathbf{x}', t) = \int_{\mathbb{S}_0} R(\mathbf{x}', \mathbf{x}'', t) * p^+(\mathbf{x}'', t) \mathrm{d}\mathbf{x}'', \qquad (24)$$

for $\mathbf{x}'$ and $\mathbf{x}''$ at $\mathbb{S}_0$. We consider a dipole source in the homogeneous upper half-space at $\mathbf{x}_D = (\mathbf{x}_{H,D}, z_0 - \epsilon)$ (with $\mathbf{x}_{H,D}$ denoting the horizontal component(s) of $\mathbf{x}_D$), at a vanishing distance ϵ above $\mathbb{S}_0$. This is the source for the wave field $p(\mathbf{x}, t)$. We scale it such that for the downgoing field at $\mathbf{x}''$ on $\mathbb{S}_0$ we have

$$p^+(\mathbf{x}'', t) = \delta(\mathbf{x}''_H - \mathbf{x}_{H,D}) s(t), \qquad (25)$$

where $s(t)$ is the source wavelet. Substitution of Equation (25) into Equation (24) gives

$$p^-(\mathbf{x}', t) = R(\mathbf{x}', \mathbf{x}_D, t) * s(t), \qquad (26)$$

for $\mathbf{x}'$ at $\mathbb{S}_0$. Substitution of Equations (25) and (26) into Equation (23) yields

$$p(\mathbf{x}, t) = \int_{\mathbb{S}_0} F(\mathbf{x}, \mathbf{x}', t) * R(\mathbf{x}', \mathbf{x}_D, t) * s(t) \mathrm{d}\mathbf{x}'$$
$$+ F(\mathbf{x}, \mathbf{x}_D, -t) * s(t). \qquad (27)$$

Since the source at $\mathbf{x}_D$ lies just above $\mathbb{S}_0$, this expression holds only for $\mathbf{x}$ at and below $\mathbb{S}_0$. First, we evaluate a discretized version of only the first term on the right-hand side of Equation (27), that is,

$$\sum_{n=-N}^{N} F(\mathbf{x}, \mathbf{x}_n, t) * R(\mathbf{x}_n, \mathbf{x}_D, t) * s(t), \qquad (28)$$

with $\mathbf{x}_n = (n\Delta x, z_0)$, $\Delta x = 200$ m and $N = 50$. For this 2D example, we choose $\mathbf{x}_{H,D} = x_D = 0$. The result is shown in Figure 12a–d, for $t = 0.2$ s, $t = 0.6$ s, $t = 1.0$ s and $t = 1.4$ s, respectively. The envelopes of the superposed waves converge to wave fronts, but it is not yet obvious how they are connected to the desired response $p(\mathbf{x}, t)$ (which is the response to a dipole source at $\mathbf{x}_D$). Next, we replace the summation by an integration and we add the term $F(\mathbf{x}, \mathbf{x}_D, -t) * s(t)$, that is, we add Figure 9c, 9b and 9a to the converged versions of Figure 12a, 12b and 12c. The results are shown in Figure 13. This figure clearly shows the desired response to the dipole source at $\mathbf{x}_D$, observed at all $\mathbf{x}$ in the lower half-space, including internal multiply reflected waves (compare Figure 13a and 13d with the directly modelled dipole Green's function in the lower half-space in Figure 5a and 5b at $t = 0.2$ s and $t = 1.4$ s, respectively).

Extrapolation of reflection data with focusing functions finds applications in acoustic and seismic imaging schemes, accounting for internal multiply reflected waves (Ravasi et al. 2016; Jia et al. 2018; Staring and Wapenaar 2020; Brackenhoff et al. 2022). In those applications, the focusing functions are obtained with the Marchenko method from numerically modelled or field reflection responses of 2D and 3D inhomogeneous media. The focal points of those focusing functions are inside the medium, but, as long as evanescent waves can be neglected, they are straightforwardly related to focusing functions with their focal points at $\mathbb{S}_0$ (Wapenaar et al. 2014).
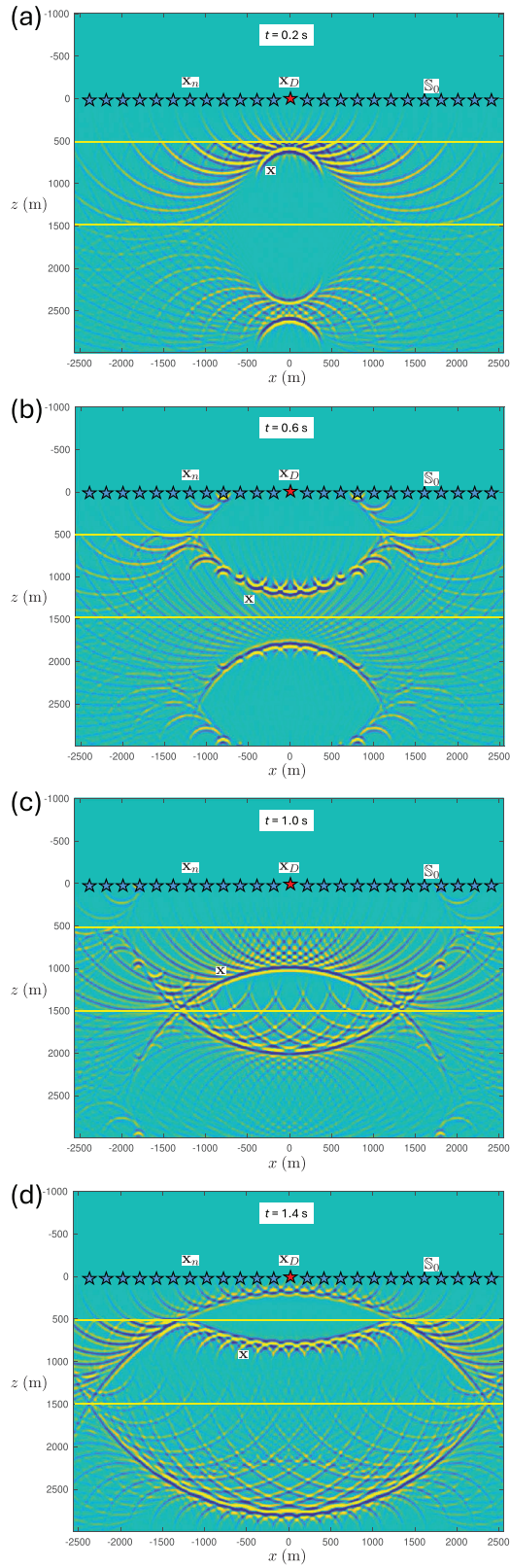
Figure 12 │ Illustration of the first term of the modified Huygens' principle (Equation 28, with the focusing function of Figure 9), applied to the discretized reflection response $R(\mathbf{x}_n, \mathbf{x}_D, t) * s(t)$.
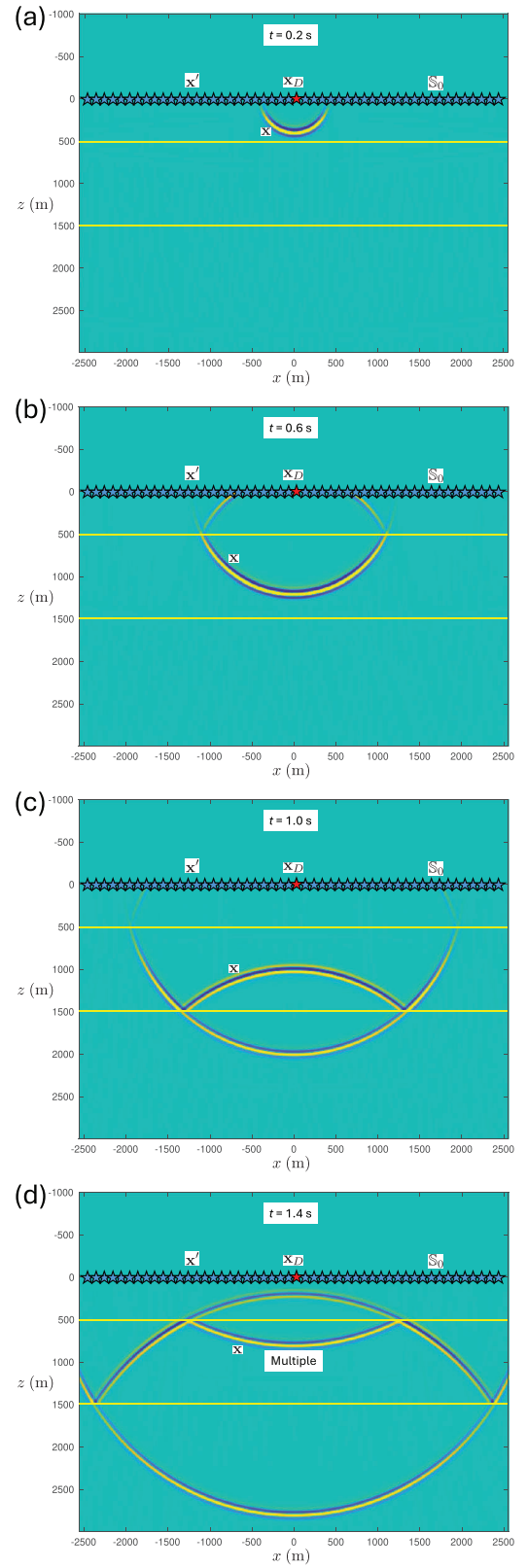
Figure 13 │ Illustration of the modified Huygens' principle (both terms of Equation 27), applied to the continuous reflection response $R(\mathbf{x}', \mathbf{x}_D, t) * s(t)$.
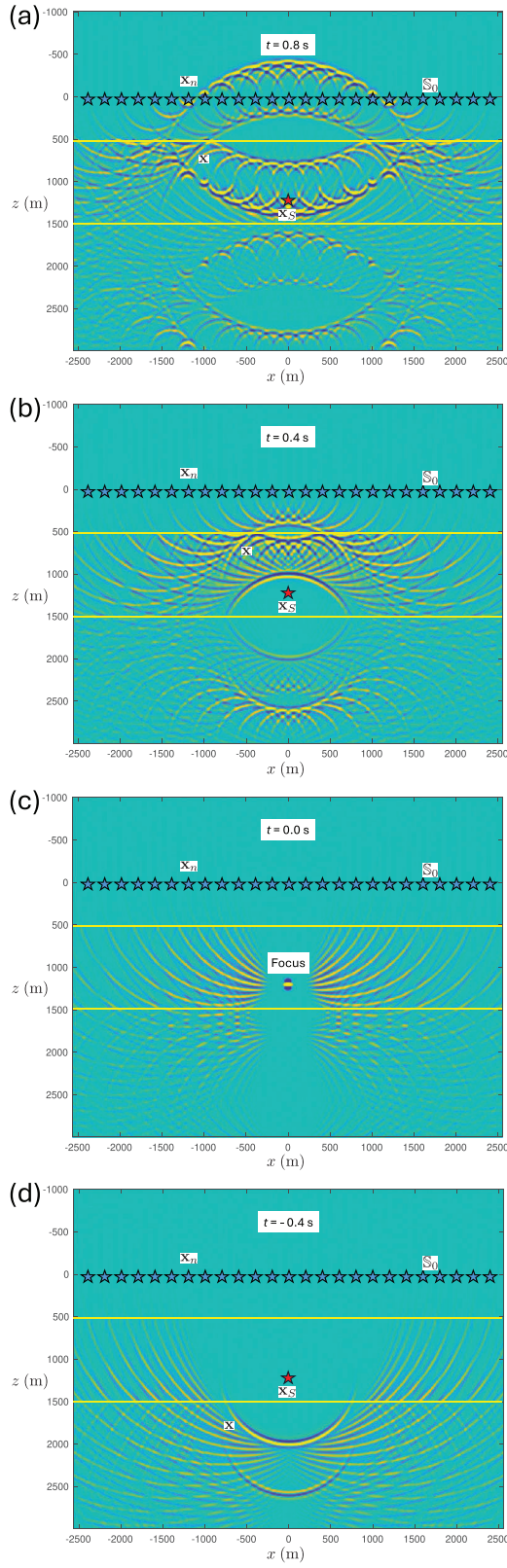
Figure 14 | Illustration of the first term of the modified Huygens' principle (Equation 30, with the focusing function of Figure 9), applied to the discretized Green's function $G(\mathbf{x}_n, \mathbf{x}_S, t)$.
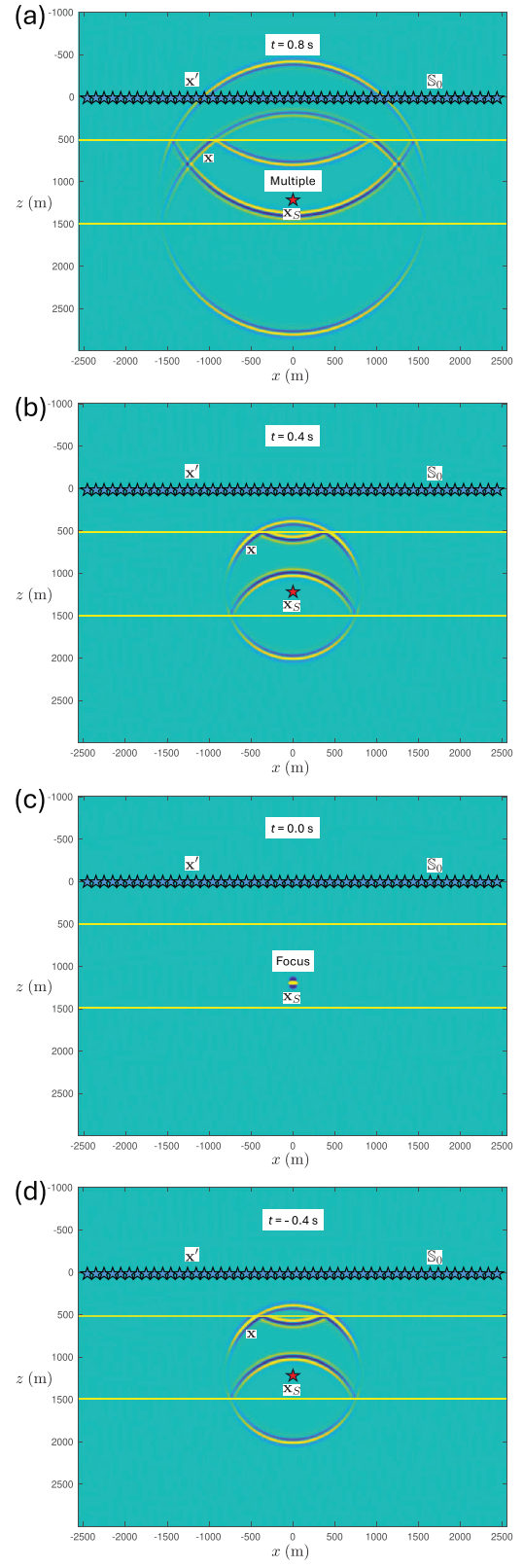
Figure 15 | Illustration of the modified Huygens' principle (both terms of Equation 29), applied to the continuous Green's function $G(\mathbf{x}', \mathbf{x}_S, t)$ and its time-reversal $G(\mathbf{x}', \mathbf{x}_S, -t)$.

3.6 | Retrieval of the Homogeneous Green's Function in an Inhomogeneous Medium

In Equation (16), we introduced the homogeneous Green's function $G_{\mathrm{h}}(\mathbf{x}, \mathbf{x}_S, t) = G(\mathbf{x}, \mathbf{x}_S, t) + G(\mathbf{x}, \mathbf{x}_S, -t)$ for an inhomogeneous lossless medium. Both terms on the right-hand side obey a wave equation with a source at $\mathbf{x}_S$, but these sources cancel each other, implying that the wave equation for $G_{\mathrm{h}}(\mathbf{x}, \mathbf{x}_S, t)$ is source-free (see Appendix A2). Hence, when in Equation (23) we replace $p(\mathbf{x}, t)$ by $G_{\mathrm{h}}(\mathbf{x}, \mathbf{x}_S, t)$, it will hold throughout space, independent of the position of $\mathbf{x}_S$. With this replacement, the upgoing and downgoing wave fields $p^-(\mathbf{x}', t)$ and $p^+(\mathbf{x}', t)$ on the right-hand side of Equation (23) need to be replaced by $G_{\mathrm{h}}^-(\mathbf{x}', \mathbf{x}_S, t)$ and $G_{\mathrm{h}}^+(\mathbf{x}', \mathbf{x}_S, t)$, respectively. Assuming again that $\mathbf{x}_S$ lies below $\mathbb{S}_0$, taking into account that $\mathbf{x}'$ is situated at $\mathbb{S}_0$ and that the half-space above $\mathbb{S}_0$ is homogeneous, it follows that the Green's function $G(\mathbf{x}', \mathbf{x}_S, t)$ propagates upward for $\mathbf{x}'$ at $\mathbb{S}_0$ (see Figure 4). As a result, the time-reversed Green's function $G(\mathbf{x}', \mathbf{x}_S, -t)$ propagates downward for $\mathbf{x}'$ at $\mathbb{S}_0$. Since these two terms constitute the total homogeneous Green's function, it follows that $G_{\mathrm{h}}^-(\mathbf{x}', \mathbf{x}_S, t) = G(\mathbf{x}', \mathbf{x}_S, t)$ and $G_{\mathrm{h}}^+(\mathbf{x}', \mathbf{x}_S, t) = G(\mathbf{x}', \mathbf{x}_S, -t)$ for $\mathbf{x}'$ at $\mathbb{S}_0$. With these substitutions, Equation (23) becomes

$$
\begin{aligned}
G_{\mathrm{h}}(\mathbf{x}, \mathbf{x}_S, t) = &\int_{\mathbb{S}_0} F(\mathbf{x}, \mathbf{x}', t) * G(\mathbf{x}', \mathbf{x}_S, t)\mathrm{d}\mathbf{x}' \\
&+ \int_{\mathbb{S}_0} F(\mathbf{x}, \mathbf{x}', -t) * G(\mathbf{x}', \mathbf{x}_S, -t)\mathrm{d}\mathbf{x}', \quad (29)
\end{aligned}
$$

for all $\mathbf{x}$ throughout space. Compare this with Equation (17), where the two integrals are taken over two different boundaries. In Equation (29), both integrals are taken over the same boundary. Moreover, the second integral is merely the time-reversal of the first integral.

We illustrate Equation (29) for the same layered medium as in the previous examples and with $\mathbf{x}_S = (0, 1200)$ m. First, we evaluate a discretized version of only the first term on the right-hand side of Equation (29), that is,

$$
\sum_{n=-N}^{N} F(\mathbf{x}, \mathbf{x}_n, t) * G(\mathbf{x}_n, \mathbf{x}_S, t), \quad (30)
$$

with $\mathbf{x}_n = (n\Delta x, z_0)$, $\Delta x = 200$ m, $N = 50$, and with $G(\mathbf{x}_n, \mathbf{x}_S, t)$ tapered at large propagation angles. The result is shown in Figure 14a–d, for $t = 0.8$ s, $t = 0.4$ s, $t = 0.0$ s and $t = -0.4$ s, respectively. Next, we replace the summation by an integration and (following Equation 29), we add its time-reversal, that is, we superpose the converged versions of Figure 14b (at $t = 0.4$ s) and 14d (at $t = -0.4$ s), etc. The result is shown in Figure 15. This figure shows the retrieved homogeneous Green's function $G_{\mathrm{h}}(\mathbf{x}, \mathbf{x}_S, t)$. Note that the result in Figure 15 is indistinguishable from that in Figure 7. However, whereas Figure 7 was obtained from an integral over two boundaries, using the traditional Huygens' principle with time-reversed dipole Green's functions, Figure 15 is the result of an integral over a single boundary and

its time-reversal, using the modified Huygens' principle with focusing functions.

Retrieval of the homogeneous Green's function from wave field observations at a single boundary finds applications in holographic imaging and inverse scattering (Wapenaar et al. 2016; Diekmann and Vasconcelos 2021) and in monitoring of induced acoustic (Van der Neut et al. 2017) and seismic sources (Brackenhoff et al. 2019). In those applications, the focusing functions are obtained with the Marchenko method from numerically modelled or field reflection responses of 2D inhomogeneous media.

4 | Conclusions

Huygens' principle stands as a milestone in the history of wave theory. Originally formulated to explain the propagation of light, it has found many applications in optics, acoustics, geophysics, etc. Central in the mathematical formulation of Huygens' principle, due to 19th century physicists Fresnel, Kirchhoff, Helmholtz, Rayleigh and others, is the Green's function, which formalizes the responses to the secondary sources in Huygens' principle. Many of the present-day applications of Huygens' principle use time-reversed Green's functions. These time-reversed Green's functions are acausal and as such do not describe physical responses to secondary sources. However, they play a fundamental role in algorithms for backpropagation, imaging, inversion, seismic interferometry, etc.

We have demonstrated with numerical examples that the traditional Huygens' principle with time-reversed Green's functions has limitations when the medium is inhomogeneous. In particular, when measurements are available only at a single boundary, internal multiply reflected waves are incorrectly handled. To remedy this, Huygens' principle has been modified by replacing the Green's functions by focusing functions. For a homogeneous medium, this replacement does not make much difference but for an inhomogeneous medium the improvement is considerable. Using the modified Huygens' principle with focusing functions, the limitations of the traditional Huygens' principle with time-reversed Green's functions are evaded. This has been demonstrated with numerical examples for a simple horizontally layered medium, but note that the modified principle holds for an arbitrary inhomogeneous medium. The only assumption is that evanescent waves can be ignored at the boundary. No assumptions are made about up-down decomposition inside the inhomogeneous lower half-space.

Similar to the time-reversed Green's functions in Huygens' principle, the focusing functions in the modified Huygens' principle do not describe physical responses to secondary sources. However, they play an important role in novel algorithms for acoustic and seismic imaging and inverse scattering, for monitoring of induced acoustic and seismic sources, etc. In all these cases, the focusing functions can be obtained from the reflection response

with the Marchenko method, taking internal multiply reflected waves properly into account.

References

Berkhout, A. J. 1985. *Seismic Migration. Imaging of acoustic Energy by Wave Field Extrapolation. A. Theoretical Aspects*, 3rd ed., Elsevier.

Berkhout, A. J., and C. P. A. Wapenaar. 1989. "One-Way Versions of the Kirchhoff Integral." *Geophysics* 54, no. 4: 460–467.

Bleistein, N. 1984. *Mathematical Methods for Wave Phenomena*, Academic Press.

Bojarski, N. N. 1983. "Generalized Reaction Principles and Reciprocity Theorems for the Wave Equations and the Relationship Between the Time-Advanced and Time-Retarded Fields." *Journal of the Acoustical Society of America* 74: 281–285.

Brackenhoff, J., J. Thorbecke, and K. Wapenaar. 2019. "Monitoring of Induced Distributed Double-Couple Sources Using Marchenko-Based Virtual Receivers." *Solid Earth* 10: 1301–1319.

Brackenhoff, J., J. Thorbecke, G. Meles, V. Koehne, D. Barrera, and K. Wapenaar. 2022. "3D Marchenko Applications: Implementation and Examples." *Geophysical Prospecting* 70: 35–56.

Broggini, F., and R. Snieder. 2012. "Connection of Scattering Principles: A Visual and Mathematical Tour." *European Journal of Physics* 33: 593–613.

Campillo, M., and A. Paul. 2003. "Long-Range Correlations in the Diffuse Seismic Coda." *Science* 299: 547–549.

Cohen, J. K., F. G. Hagin, and N. Bleistein. 1986. "Three-Dimensional Born Inversion With An Arbitrary Reference." *Geophysics* 51: 1552–1558.

Corones, J. P. 1975. "Bremmer Series That Correct Parabolic Approximations." *Journal of Mathematical Analysis and Applications* 50: 361–372.

Diekmann, L., and I. Vasconcelos. 2021. "Focusing and Green's Function Retrieval in Three-Dimensional Inverse Scattering Revisited: A Single-Sided Marchenko Integral for the Full Wave Field." *Physical Review Research* 3: 013206.

Draganov, D., X. Campman, J. Thorbecke, A. Verdel, and K. Wapenaar. 2009. "Reflection Images From Ambient Seismic Noise." *Geophysics* 74, no. 5: A63–A67.

Dukalski, M., C. Reinicke, and K. Wapenaar. 2022. "Implications of Evanescent Waves for the Marchenko Method Through the Lens of the Transfer-Scattering Matrix Relation." In *EAGE Extended Abstracts*, 1–4. European Association of Geoscientists & Engineers.

Fink, M. 1992. "Time-Reversal of Ultrasonic Fields: Basic Principles." *IEEE Transactions on Ultrasonics, Ferroelectrics and Frequency Control* 39: 555–566.

Fishman, L., and J. J. McCoy. 1984. "Derivation and Application of Extended Parabolic Wave Theories. I. The Factorized Helmholtz Equation." *Journal of Mathematical Physics* 25, no. 2: 285–296.

Frazer, L. N., and M. K. Sen. 1985. "Kirchhoff-Helmholtz Reflection Seismograms in a Laterally Inhomogeneous Multi-Layered Elastic Medium, I, Theory." *Geophysical Journal of the Royal Astronomical Society* 80: 121–147.

Gazdag, J. 1978. "Wave Equation Migration with the Phase-Shift Method." *Geophysics* 43: 1342–1351.

Jia, X., A. Guitton, and R. Snieder. 2018. "A Practical Implementation of Subsalt Marchenko Imaging With A Gulf of Mexico Data Set." *Geophysics* 83, no. 5: S409–S419.

Kennett, B. L. N. 1983. *Seismic Wave Propagation in Stratified Media*. Cambridge University Press.

McMechan, G. A. 1983. "Migration by Extrapolation of Time-Dependent Boundary Values." *Geophysical Prospecting* 31: 413–420.

Meles, G. A., K. Löer, M. Ravasi, A. Curtis, and C. A. da Costa Filho. 2015. "Internal Multiple Prediction and Removal Using Marchenko Autofocusing and Seismic Interferometry." *Geophysics* 80, no. 1: A7–A11.

Morse, P. M., and H. Feshbach. 1953. *Methods of Theoretical Physics, Vol. I*, McGraw-Hill.

Moser, T. J., and E. A. Robinson. 2024. *Walking With Christiaan Huygens. From Archimedes' Influence to Unsung Contributions in Modern Science* Springer.

Oristaglio, M. L. 1989. "An Inverse Scattering Formula That Uses All The Data." *Inverse Problems* 5: 1097–1105.

Porter, R. P. 1970. "Diffraction-Limited, Scalar Image Formation With Holograms of Arbitrary Shape." *Journal of the Optical Society of America* 60: 1051–1059.

Ravasi, M., I. Vasconcelos, A. Kritski, A. Curtis, C. A. da Costa Filho, and G. A. Meles. 2016. "Target-Oriented Marchenko Imaging of a North Sea Field." *Geophysical Journal International* 205: 99–104.

Rayleigh, J. W. S. 1878. *The Theory of Sound. Volume II*. Dover. (Reprint 1945).

Roux, P., W. A. Kuperman, and the NPAL Group. 2004. "Extracting Coherent Wave Fronts from Acoustic Ambient Noise in the Ocean." *Journal of the Acoustical Society of America* 116: 1995–2003.

Sabra, K. G., S. Conti, P. Roux, and W. A. Kuperman. 2007. "Passive *In Vivo* Elastography From Skeletal Muscle Noise." *Applied Physics Letters* 90: 194101.

Schneider, W. A. 1978. "Integral Formulation for Migration in Two and Three Dimensions." *Geophysics* 43: 49–76.

Schuster, G. T., J. Yu, J. Sheng, and J. Rickett. 2004. "Interferometric/Daylight Seismic Imaging." *Geophysical Journal International* 157: 838–852.

Slob, E., K. Wapenaar, F. Broggini, and R. Snieder. 2014. "Seismic Reflector Imaging Using Internal Multiples With Marchenko-Type Equations." *Geophysics* 79, no. 2: S63–S76.

Snieder, R. 2004. "Extracting the Green's Function From the Correlation of Coda Waves: A Derivation Based on Stationary Phase." *Physical Review E* 69: 046610.

Staring, M., and K. Wapenaar. 2020. "Three-Dimensional Marchenko Internal Multiple Attenuation on Narrow Azimuth Streamer Data of the Santos Basin, Brazil." *Geophysical Prospecting* 68: 1864–1877.

Tygel, M., J. Schleicher, L. T. Santos, and P. Hubral. 2000. "An Asymptotic Inverse to the Kirchhoff-Helmholtz Integral." *Inverse Problems* 16: 425–445.

Ursin, B. 1983. "Review of Elastic and Electromagnetic Wave Propagation in Horizontally Layered Media." *Geophysics* 48: 1063–1081.

van der Neut, J., I. Vasconcelos, and K. Wapenaar. 2015. "On Green's Function Retrieval by Iterative Substitution of the Coupled Marchenko Equations." *Geophysical Journal International* 203: 792–813.

van der Neut, J., J. L. Johnson, K. van Wijk, S. Singh, E. Slob, and K. Wapenaar. 2017. "A Marchenko Equation for Acoustic Inverse Source Problems." *Journal of the Acoustical Society of America* 141, no. 6: 4332–4346.

Wapenaar, C. P. A., G. L. Peels, V. Budejicky, and A. J. Berkhout. 1989. "Inverse Extrapolation of Primary Seismic Waves." *Geophysics* 54, no. 7: 853–863.

Wapenaar, K., and J. Fokkema. 2006. "Green's Function Representations for Seismic Interferometry." *Geophysics* 71, no. 4: SI33–SI46.

Wapenaar, K., J. Thorbecke, J. van der Neut, F. Broggini, E. Slob, and R. Snieder. 2014. "Marchenko Imaging." *Geophysics* 79, no 3: WA39–WA57.

Wapenaar, K., J. van der Neut, and E. Slob. 2016. "Unified Double-and Single-Sided Homogeneous Green's Function Representations." *Proceedings of the Royal Society A* 472: 20160162.

Wapenaar, K., R. Snieder, S. de Ridder, and E. Slob. 2021. "Green's Function Representations for Marchenko Imaging Without Up/Down Decomposition." *Geophysical Journal International* 227: 184–203.

Wapenaar, K., M. Dukalski, C. Reinicke, and R. Snieder. 2023. "Propagator and Transfer Matrices, Marchenko Focusing Functions and their Mutual Relations." *Geophysical Journal International* 235: 1403–1419.

Weaver, R. L., and O. I. Lobkis. 2001. "Ultrasonics Without a Source: Thermal Fluctuation Correlations at MHz Frequencies." *Physical Review Letters* 87: 134301.

Whitmore, N. D. 1983. "Iterative depth migration by backward time propagation." In *SEG Expanded Abstracts*, 382–385. Society of Exploration Geophysicists.

Appendix A: Monopole and Dipole Green's Functions

A.1 | Monopole Green's Function

The wave equation for the acoustic pressure $p(\mathbf{x}, t)$ in an inhomogeneous lossless medium with propagation velocity $c(\mathbf{x})$ and mass density $\rho(\mathbf{x})$ reads

$$\mathcal{L}p = -\partial_t q, \tag{A.1}$$

with ∂_t standing for $\partial/\partial t$, wave operator $\mathcal{L}(\mathbf{x}, t)$ defined as

$$\mathcal{L} = \nabla \cdot \frac{1}{\rho}\nabla - \frac{1}{\rho c^2}\partial_t^2 \tag{A.2}$$

and source function $q(\mathbf{x}, t)$ being the volume-injection rate density. We define the Green's function $\mathcal{G}(\mathbf{x}, \mathbf{x}', t)$ as the solution of

$$\mathcal{L}\mathcal{G} = -\delta(\mathbf{x} - \mathbf{x}')\delta(t), \tag{A.3}$$

with $\delta(\mathbf{x}) = \delta(x)\delta(y)\delta(z)$ and causality condition

$$\mathcal{G}(\mathbf{x}, \mathbf{x}', t) = 0, \quad \text{for} \quad t < 0. \tag{A.4}$$

Hence, $\mathcal{G}(\mathbf{x}, \mathbf{x}', t)$ is the response to an impulse at $\mathbf{x}'$ and $t = 0$, observed at $\mathbf{x}$ as a function of t. Similarly, we define $G(\mathbf{x}, \mathbf{x}', t)$ as the response to an impulsive volume-injection rate source $q(\mathbf{x}, t) = \delta(\mathbf{x} - \mathbf{x}')\delta(t)$; hence, it obeys

$$\mathcal{L}G = -\delta(\mathbf{x} - \mathbf{x}')\partial_t\delta(t) \tag{A.5}$$

and a causality condition similar to Equation (A4). We apply the operator ∂_t to both sides of Equation (A3) and use the property $\partial_t\mathcal{L} = \mathcal{L}\partial_t$ (since $\rho(\mathbf{x})$ and $c(\mathbf{x})$ are independent of t). Comparing the result with Equation (A5), it follows that $G(\mathbf{x}, \mathbf{x}', t)$ and $\mathcal{G}(\mathbf{x}, \mathbf{x}', t)$ are mutually related via

$$G(\mathbf{x}, \mathbf{x}', t) = \partial_t\mathcal{G}(\mathbf{x}, \mathbf{x}', t). \tag{A.6}$$

Note that the source terms in Equations (A3) and (A5) represent monopole sources at $\mathbf{x}'$; hence, we call G and $\mathcal{G}$ monopole Green's functions.

For the special case of a homogeneous medium, we have for the 3D situation

$$\mathcal{G}(\mathbf{x}, \mathbf{x}', t) = \rho\frac{\delta(t - ||\mathbf{x} - \mathbf{x}'||/c)}{4\pi||\mathbf{x} - \mathbf{x}'||} \tag{A.7}$$

and for the 2D situation

$$\mathcal{G}(\mathbf{x}, \mathbf{x}', t) = \rho\frac{H(t - ||\mathbf{x} - \mathbf{x}'||/c)}{2\pi\sqrt{t^2 - ||\mathbf{x} - \mathbf{x}'||^2/c^2}}, \tag{A.8}$$

where $H(t)$ is the Heaviside function. According to Equation (A6), explicit expressions for $G(\mathbf{x}, \mathbf{x}', t)$ in a homogeneous medium are obtained by taking the time-derivative of the expressions in the right-hand sides of Equations (A7) and (A8).

A.2 | Homogeneous Green's Function

We consider again an inhomogeneous lossless medium, with propagation velocity $c(\mathbf{x})$ and mass density $\rho(\mathbf{x})$. Since operator $\mathcal{L}$, defined in Equation (A2), contains only even order time-derivatives and the source term in wave equation (A3) is an even function of time, the time-reversed Green's function $\mathcal{G}(\mathbf{x}, \mathbf{x}', -t)$ also obeys this wave equation. We define the homogeneous Green's function $\mathcal{G}_h(\mathbf{x}, \mathbf{x}', t)$ as

$$\mathcal{G}_h(\mathbf{x}, \mathbf{x}', t) = \mathcal{G}(\mathbf{x}, \mathbf{x}', t) - \mathcal{G}(\mathbf{x}, \mathbf{x}', -t) \tag{A.9}$$

(Porter 1970; Oristaglio 1989). Since Equation (A3) holds for both terms in the right-hand side of Equation (A9), their difference obeys the homogeneous differential equation $\mathcal{L}\mathcal{G}_h = 0$ (hence the name 'homogeneous Green's function' for $\mathcal{G}_h$).

Since the source term in wave equation (A5) is an odd function of time, the opposite time-reversed Green's function $-G(\mathbf{x}, \mathbf{x}', -t)$ also obeys this wave equation. Hence, the homogeneous Green's function $G_h(\mathbf{x}, \mathbf{x}', t)$, defined as

$$G_h(\mathbf{x}, \mathbf{x}', t) = G(\mathbf{x}, \mathbf{x}', t) + G(\mathbf{x}, \mathbf{x}', -t), \tag{A.10}$$

obeys the homogeneous differential equation $\mathcal{L}G_h = 0$. From Equation (A6) and the definitions of $\mathcal{G}_h$ and G_h, it follows that these homogeneous Green's functions are mutually related via

$$G_h(\mathbf{x}, \mathbf{x}', t) = \partial_t\mathcal{G}_h(\mathbf{x}, \mathbf{x}', t). \tag{A.11}$$

A.3 | Dipole Green's Function

Next, we define a Green's function $G_d(\mathbf{x}, \mathbf{x}', t)$ as the solution of

$$\mathcal{L}G_d = \frac{1}{\rho(\mathbf{x}')}\partial_z\delta(\mathbf{x} - \mathbf{x}')\delta(t), \tag{A.12}$$

with a causality condition similar to Equation (A4) and ∂_z standing for $\partial/\partial z$. Note that

$$\partial_z\delta(z - z') = \lim_{\Delta z \to 0}\frac{\delta(z + \frac{\Delta z}{2} - z') - \delta(z - \frac{\Delta z}{2} - z')}{\Delta z}. \tag{A.13}$$

Hence, the right-hand side of Equation (A12) represents a vertically oriented dipole source at $\mathbf{x}'$. Therefore, we call G_d a dipole Green's function. We define ∂_z' as an operator for differentiation with respect to z'. We apply this operator to both sides of Equation (A3) and use the properties $\partial_z'\mathcal{L} = \mathcal{L}\partial_z'$ (since $\rho(\mathbf{x})$ and $c(\mathbf{x})$ are independent of z') and $\partial_z'\delta(z - z') = -\partial_z\delta(z - z')$. Comparing the result with Equation (A12), it follows that $G_d(\mathbf{x}, \mathbf{x}', t)$ and $\mathcal{G}(\mathbf{x}, \mathbf{x}', t)$ are mutually related via

$$G_d(\mathbf{x}, \mathbf{x}', t) = \frac{1}{\rho(\mathbf{x}')}\partial_z'\mathcal{G}(\mathbf{x}, \mathbf{x}', t). \tag{A.14}$$

Appendix B: Forward Wave Field Extrapolation

We define the temporal Fourier transform of a space- and time-dependent quantity $p(\mathbf{x}, t)$ as

$$\hat{p}(\mathbf{x}, \omega) = \int_{-\infty}^{\infty} p(\mathbf{x}, t) \exp(i\omega t) \mathrm{d}t, \qquad (B.1)$$

where i is the imaginary unit and ω the angular frequency (we consider positive ω only). With this definition, differentiation with respect to t in the time domain is replaced by multiplication with $-i\omega$ in the frequency domain; hence, wave equations (A1) and (A3) transform to

$$\hat{\mathcal{L}}\hat{p} = i\omega\hat{q} \qquad (B.2)$$

and

$$\hat{\mathcal{L}}\hat{\mathcal{G}} = -\delta(\mathbf{x} - \mathbf{x}'), \qquad (B.3)$$

respectively, with operator $\hat{\mathcal{L}}(\mathbf{x}, \omega)$ defined as

$$\hat{\mathcal{L}} = \boldsymbol{\nabla} \cdot \frac{1}{\rho}\boldsymbol{\nabla} + \frac{\omega^2}{\rho c^2}. \qquad (B.4)$$

Consider the quantity $\boldsymbol{\nabla} \cdot \{\hat{\mathcal{G}}(\frac{1}{\rho}\boldsymbol{\nabla}\hat{p}) - \hat{p}(\frac{1}{\rho}\boldsymbol{\nabla}\hat{\mathcal{G}})\}$, apply the product rule for differentiation and simplify the result using wave equations (B2) and (B3). This yields

$$\boldsymbol{\nabla} \cdot \{\hat{\mathcal{G}}\frac{1}{\rho}\boldsymbol{\nabla}\hat{p} - \hat{p}\frac{1}{\rho}\boldsymbol{\nabla}\hat{\mathcal{G}}\} = i\omega\hat{\mathcal{G}}\hat{q} + \hat{p}\delta(\mathbf{x} - \mathbf{x}'). \qquad (B.5)$$

Integrate both sides of this equation over a domain $\mathbb{V}$ with boundary $\mathbb{S}$ and outward pointing normal vector $\mathbf{n}$ and apply the theorem of Gauss to the left-hand side. Use the source–receiver reciprocity relation $\hat{\mathcal{G}}(\mathbf{x}, \mathbf{x}', \omega) = \hat{\mathcal{G}}(\mathbf{x}', \mathbf{x}, \omega)$ and subsequently modify the notation by replacing all $\mathbf{x}$ by $\mathbf{x}'$ and vice versa (meaning that effectively $\hat{\mathcal{G}}(\mathbf{x}, \mathbf{x}', \omega)$ remains unchanged). This yields the Kirchhoff–Helmholtz integral representation (Morse and Feshbach 1953; Bleistein 1984)

$$\chi_{\mathbb{V}}(\mathbf{x})\hat{p}(\mathbf{x}, \omega) = \oint_{\mathbb{S}} \frac{1}{\rho(\mathbf{x}')}\Big(\hat{\mathcal{G}}(\mathbf{x}, \mathbf{x}', \omega)\boldsymbol{\nabla}'\hat{p}(\mathbf{x}', \omega)$$

$$- \hat{p}(\mathbf{x}', \omega)\boldsymbol{\nabla}'\hat{\mathcal{G}}(\mathbf{x}, \mathbf{x}', \omega)\Big) \cdot \mathbf{n}\mathrm{d}\mathbf{x}'$$

$$- \int_{\mathbb{V}} i\omega\hat{\mathcal{G}}(\mathbf{x}, \mathbf{x}', \omega)\hat{q}(\mathbf{x}', \omega)\mathrm{d}\mathbf{x}', \qquad (B.6)$$

with operator $\boldsymbol{\nabla}'$ acting on $\mathbf{x}'$ and $\chi_{\mathbb{V}}(\mathbf{x})$ being the characteristic function for $\mathbb{V}$, defined as

$$\chi_{\mathbb{V}}(\mathbf{x}) = \begin{cases} 1 & \text{for} \quad \mathbf{x} \text{ in } \mathbb{V}, \\ \frac{1}{2} & \text{for} \quad \mathbf{x} \text{ on } \mathbb{S}, \\ 0 & \text{for} \quad \mathbf{x} \text{ outside } \mathbb{V} \cup \mathbb{S}. \end{cases} \qquad (B.7)$$

We use Equation (B6) to derive an expression for forward wave field extrapolation in the configuration of Figure B1 (Berkhout 1985; Frazer and Sen 1985). The closed boundary $\mathbb{S}$ consists of an infinite horizontal boundary $\mathbb{S}_0$ (at $z = z_0$) and a half-sphere $\mathbb{S}_{\mathrm{sph}}$ with infinite radius ($r \to \infty$) in the upper half-space (above $\mathbb{S}_0$). The upper half-space is homogeneous; the lower half-space may be inhomogeneous. We choose the source distribution $\hat{q}(\mathbf{x}', \omega)$ in the lower half-space (below $\mathbb{S}_0$) hence outside $\mathbb{V}$. This implies that the volume integral on the right-hand side of Equation (B6) vanishes. The boundary integral over the half-sphere with infinite radius also vanishes (Sommerfeld radiation condition). Hence, we are left with a boundary integral over $\mathbb{S}_0$. At this boundary, the outward pointing normal vector $\mathbf{n}$ equals $(0,0,1)$; hence, $\boldsymbol{\nabla}' \cdot \mathbf{n} = \partial_z'$ at $\mathbb{S}_0$. Using
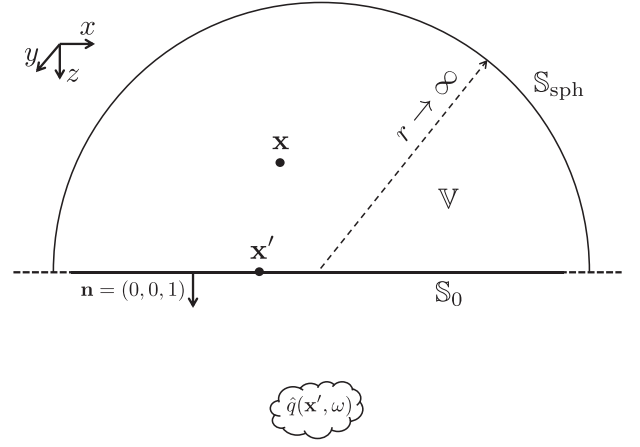

Figure B.1 │ Configuration for forward wave field extrapolation (side view).

the equation of motion $\frac{1}{\rho(\mathbf{x}')}\partial_z'\hat{p}(\mathbf{x}', \omega) = i\omega\hat{v}_z(\mathbf{x}', \omega)$, where $\hat{v}_z$ is the vertical component of the particle velocity, and the Fourier transforms of Equations (A6) and (A14), we thus obtain

$$\chi_{\mathbb{V}}(\mathbf{x})\hat{p}(\mathbf{x}, \omega) = -\int_{\mathbb{S}_0} \Big(\hat{G}(\mathbf{x}, \mathbf{x}', \omega)\hat{v}_z(\mathbf{x}', \omega)$$

$$+ \hat{G}_{\mathrm{d}}(\mathbf{x}, \mathbf{x}', \omega)\hat{p}(\mathbf{x}', \omega)\Big)\mathrm{d}\mathbf{x}'. \qquad (B.8)$$

For $\mathbf{x}$ in the lower half-space, we have $\chi_{\mathbb{V}}(\mathbf{x}) = 0$; hence, the integral on the right-hand side vanishes for this situation. For $\mathbf{x}$ in the upper half-space, we have $\chi_{\mathbb{V}}(\mathbf{x}) = 1$; hence, for this situation, Equation (B8) describes forward wave field extrapolation from the horizontal boundary $\mathbb{S}_0$ to any point $\mathbf{x}$ above this boundary. Since the upper half-space is homogeneous, the actual wave field ($\hat{p}$ and $\hat{v}_z$) is upward propagating at $\mathbb{S}_0$. Taking the entire medium homogeneous for the Green's functions ($\hat{G}$ and $\hat{G}_{\mathrm{d}}$), then the two terms under the integral give equal contributions; hence, Equation (B8) can be replaced by

$$\hat{p}(\mathbf{x}, \omega) = -2\int_{\mathbb{S}_0} \hat{G}_{\mathrm{d}}(\mathbf{x}, \mathbf{x}', \omega)\hat{p}(\mathbf{x}', \omega)\mathrm{d}\mathbf{x}', \qquad (B.9)$$

for $\mathbf{x}$ in the upper half-space (Berkhout and Wapenaar 1989). Equation (B9) is a Rayleigh integral (Rayleigh (1878) derived expressions like this to describe the radiation of sources, distributed over a plane). Transforming this back to the time domain and using the causality condition of the Green's function gives

$$p(\mathbf{x}, t) = -2\int_{\mathbb{S}_0} \int_0^{\infty} G_{\mathrm{d}}(\mathbf{x}, \mathbf{x}', t')p(\mathbf{x}', t - t')\mathrm{d}t'\mathrm{d}\mathbf{x}', \qquad (B.10)$$

for $\mathbf{x}$ in the upper half-space. The time integral in this expression is a convolution, which can be written in a shorter notation using the convolution symbol $*$. Equation (B10) thus becomes

$$p(\mathbf{x}, t) = -2\int_{\mathbb{S}_0} G_{\mathrm{d}}(\mathbf{x}, \mathbf{x}', t) * p(\mathbf{x}', t)\mathrm{d}\mathbf{x}', \qquad (B.11)$$

for $\mathbf{x}$ in the upper half-space.

Appendix C: Inverse Wave Field Extrapolation

The Fourier transform of the time-reversed Green's function $\mathcal{G}(\mathbf{x}, \mathbf{x}', -t)$ is given by $\hat{\mathcal{G}}^*(\mathbf{x}, \mathbf{x}', \omega)$, where the superscript $*$ denotes complex conjugation. Since for a lossless medium $\hat{\mathcal{G}}^*$ obeys the same wave equation as
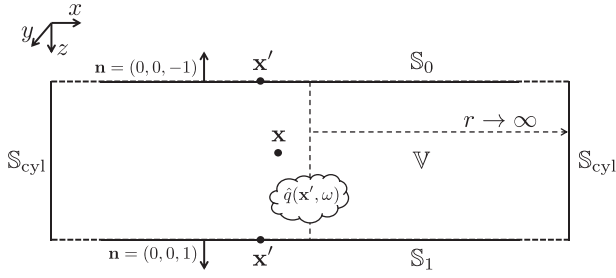
Figure C.1 | Configuration for inverse wave field extrapolation (side view).

$\hat{\mathcal{G}}$ (Equation B3), Equation (A6) remains valid when we replace $\hat{\mathcal{G}}$ by $\hat{\mathcal{G}}^*$ (Bojarski 1983), hence

$$
\begin{aligned}
\chi_{\mathbb{V}}(\mathbf{x})\hat{p}(\mathbf{x},\omega) = {} & \oint_{\mathbb{S}} \frac{1}{\rho(\mathbf{x}')} \Big(\hat{\mathcal{G}}^*(\mathbf{x},\mathbf{x}',\omega) \boldsymbol{\nabla}' \hat{p}(\mathbf{x}',\omega) \\
& - \hat{p}(\mathbf{x}',\omega) \boldsymbol{\nabla}' \hat{\mathcal{G}}^*(\mathbf{x},\mathbf{x}',\omega) \Big) \cdot \mathbf{n} \, \mathrm{d}\mathbf{x}' \\
& - \int_{\mathbb{V}} i\omega \hat{\mathcal{G}}^*(\mathbf{x},\mathbf{x}',\omega) \hat{q}(\mathbf{x}',\omega) \, \mathrm{d}\mathbf{x}'.
\end{aligned} \tag{C.1}
$$

We use Equation (C1) to derive an expression for inverse wave field extrapolation in the configuration of Figure C1. The closed boundary $\mathbb{S}$ consists of two infinite horizontal boundaries $\mathbb{S}_0$ (at $z = z_0$) and $\mathbb{S}_1$ (at $z = z_1$), connected by a cylindrical surface $\mathbb{S}_{cyl}$ with infinite radius ($r \to \infty$). The half-spaces above $\mathbb{S}_0$ and below $\mathbb{S}_1$ are homogeneous; the medium between these boundaries may be inhomogeneous. We choose the source distribution $\hat{q}(\mathbf{x}',\omega)$ between the two boundaries $\mathbb{S}_0$ and $\mathbb{S}_1$, hence inside $\mathbb{V}$. The boundary integral over the cylindrical surface with infinite radius vanishes because its surface area increases with r, but its integrand decays with $1/r^2$. The outward pointing normal vector $\mathbf{n}$ equals $(0,0,-1)$ at $\mathbb{S}_0$ and $(0,0,1)$ at $\mathbb{S}_1$; hence, $\boldsymbol{\nabla}' \cdot \mathbf{n} = -\partial_z'$ at $\mathbb{S}_0$, and $\boldsymbol{\nabla}' \cdot \mathbf{n} = \partial_z'$ at $\mathbb{S}_1$. Using again the equation of motion and the Fourier transforms of Equations (A6) and (A14), we thus obtain

$$
\begin{aligned}
\hat{p}(\mathbf{x},\omega) = {} & - \int_{\mathbb{S}_0} \Big(\hat{G}^*(\mathbf{x},\mathbf{x}',\omega) \hat{v}_z(\mathbf{x}',\omega) \\
& - \hat{G}_{\mathrm{d}}^*(\mathbf{x},\mathbf{x}',\omega) \hat{p}(\mathbf{x}',\omega) \Big) \mathrm{d}\mathbf{x}' \\
& + \int_{\mathbb{S}_1} \Big(\hat{G}^*(\mathbf{x},\mathbf{x}',\omega) \hat{v}_z(\mathbf{x}',\omega) \\
& - \hat{G}_{\mathrm{d}}^*(\mathbf{x},\mathbf{x}',\omega) \hat{p}(\mathbf{x}',\omega) \Big) \mathrm{d}\mathbf{x}' \\
& - \int_{\mathbb{V}} \hat{G}^*(\mathbf{x},\mathbf{x}',\omega) \hat{q}(\mathbf{x}',\omega) \mathrm{d}\mathbf{x}',
\end{aligned} \tag{C.2}
$$

for $\mathbf{x}$ in $\mathbb{V}$. Since the medium above $\mathbb{S}_0$ and below $\mathbb{S}_1$ is homogeneous (for the actual wave field and for the Green's function), the two terms under the boundary integrals give equal contributions; hence, Equation (C2) can be replaced by

$$
\begin{aligned}
\hat{p}(\mathbf{x},\omega) = {} & 2 \int_{\mathbb{S}_0} \hat{G}_{\mathrm{d}}^*(\mathbf{x},\mathbf{x}',\omega) \hat{p}(\mathbf{x}',\omega) \mathrm{d}\mathbf{x}' \\
& - 2 \int_{\mathbb{S}_1} \hat{G}_{\mathrm{d}}^*(\mathbf{x},\mathbf{x}',\omega) \hat{p}(\mathbf{x}',\omega) \mathrm{d}\mathbf{x}' \\
& - \int_{\mathbb{V}} \hat{G}^*(\mathbf{x},\mathbf{x}',\omega) \hat{q}(\mathbf{x}',\omega) \mathrm{d}\mathbf{x}',
\end{aligned} \tag{C.3}
$$

for $\mathbf{x}$ in $\mathbb{V}$. Going from Equation (C2) to Equation (C3), it is assumed that evanescent waves at $\mathbb{S}_0$ and $\mathbb{S}_1$ can be ignored (Wapenaar et al. 1989). Transforming Equation (C3) back to the time domain and choosing a point source $q(\mathbf{x}',t) = \delta(\mathbf{x}' - \mathbf{x}_S)s(t)$ (with $\mathbf{x}_S$ in $\mathbb{V}$) gives

$$
\begin{aligned}
p(\mathbf{x},t) = {} & 2 \int_{\mathbb{S}_0} G_{\mathrm{d}}(\mathbf{x},\mathbf{x}',-t) * p(\mathbf{x}',t) \mathrm{d}\mathbf{x}' \\
& - 2 \int_{\mathbb{S}_1} G_{\mathrm{d}}(\mathbf{x},\mathbf{x}',-t) * p(\mathbf{x}',t) \mathrm{d}\mathbf{x}' \\
& - G(\mathbf{x},\mathbf{x}_S,-t) * s(t),
\end{aligned} \tag{C.4}
$$

for $\mathbf{x}$ in $\mathbb{V}$. Inverse extrapolation is often approximated by the first term only (Schneider 1978; Berkhout 1985); hence,

$$
\langle p(\mathbf{x},t) \rangle = 2 \int_{\mathbb{S}_0} G_{\mathrm{d}}(\mathbf{x},\mathbf{x}',-t) * p(\mathbf{x}',t) \mathrm{d}\mathbf{x}', \tag{C.5}
$$

or, writing the integrand as a correlation integral,

$$
\langle p(\mathbf{x},t) \rangle = 2 \int_{\mathbb{S}_0} \int_0^\infty G_{\mathrm{d}}(\mathbf{x},\mathbf{x}',t') p(\mathbf{x}',t+t') \mathrm{d}t' \mathrm{d}\mathbf{x}', \tag{C.6}
$$

for $\mathbf{x}$ below $\mathbb{S}_0$ and above the source; see the main text for a further discussion.

Appendix D: Extrapolation With Focusing Functions

Consider a configuration, consisting of an inhomogeneous lossless medium below $\mathbb{S}_0$ (at $z = z_0$), with propagation velocity $c(\mathbf{x})$ and mass density $\rho(\mathbf{x})$, and a homogeneous lossless medium at and above $\mathbb{S}_0$, with propagation velocity c_0 and mass density ρ_0. In the space-frequency domain, the acoustic pressure $\hat{p}(\mathbf{x},\omega)$ in this configuration obeys the wave equation (B2), with operator $\hat{\mathcal{L}}(\mathbf{x},\omega)$ defined in Equation (B4). In the following, we assume that the source distribution $\hat{q}(\mathbf{x},\omega)$ is restricted to the upper half-space. Hence, for all $\mathbf{x}$ below the source distribution, $\hat{p}(\mathbf{x},\omega)$ obeys the source-free wave equation

$$
\hat{\mathcal{L}}\hat{p} = 0. \tag{D.1}
$$

For the same configuration, we define the Fourier-transformed focusing function $\hat{F}(\mathbf{x},\mathbf{x}',\omega)$, with $\mathbf{x}'$ denoting a focal point at $\mathbb{S}_0$ (hence, $z' = z_0$). This focusing function obeys the same source-free wave equation throughout space, hence

$$
\hat{\mathcal{L}}\hat{F} = 0. \tag{D.2}
$$

Moreover, $\hat{F}(\mathbf{x},\mathbf{x}',\omega)$ is defined such that for $\mathbf{x}$ at $\mathbb{S}_0$ it obeys the Fourier transform of the focusing condition of Equation (20), hence

$$
\hat{F}(\mathbf{x}_{\mathrm{H}},z_0,\mathbf{x}_{\mathrm{H}}',z_0,\omega) = \delta(\mathbf{x}_{\mathrm{H}} - \mathbf{x}_{\mathrm{H}}'), \tag{D.3}
$$

with $\mathbf{x}_{\mathrm{H}}$ and $\mathbf{x}_{\mathrm{H}}'$ being the horizontal components of $\mathbf{x}$ and $\mathbf{x}'$, respectively. Finally, for $\mathbf{x}$ at and above $\mathbb{S}_0$ this focusing function propagates upward. Note that $\hat{F}^*(\mathbf{x},\mathbf{x}',\omega)$, which is the Fourier transform of the time-reversed focusing function, obeys the same wave equation and the same focusing condition as $\hat{F}(\mathbf{x},\mathbf{x}',\omega)$; for $\mathbf{x}$ at and above $\mathbb{S}_0$ it propagates downward.

For all $\mathbf{x}$ below the source distribution, we write $\hat{p}(\mathbf{x},\omega)$ as a superposition of the mutually independent focusing functions, according to

$$
\begin{aligned}
\hat{p}(\mathbf{x},\omega) = {} & \int_{\mathbb{S}_0} \hat{F}(\mathbf{x},\mathbf{x}',\omega) \hat{a}(\mathbf{x}',\omega) \mathrm{d}\mathbf{x}' \\
& + \int_{\mathbb{S}_0} \hat{F}^*(\mathbf{x},\mathbf{x}',\omega) \hat{b}(\mathbf{x}',\omega) \mathrm{d}\mathbf{x}',
\end{aligned} \tag{D.4}
$$

where $\hat{a}(\mathbf{x}', \omega)$ and $\hat{b}(\mathbf{x}', \omega)$ are coefficients which still need to be determined. In the main text, we use physical arguments to show that these coefficients are the upgoing and downgoing parts of the wave field at $\mathbb{S}_0$. Here we show this via a more formal derivation. Using the equation of motion, we obtain a similar expression for the vertical component of the particle velocity from Equation (D4), according to

$$
\hat{v}_z(\mathbf{x}, \omega) = \frac{1}{i\omega\rho(\mathbf{x})} \partial_z \hat{p}(\mathbf{x}, \omega)
$$

$$
= \frac{1}{i\omega\rho(\mathbf{x})} \int_{\mathbb{S}_0} \partial_z \hat{F}(\mathbf{x}, \mathbf{x}', \omega) \hat{a}(\mathbf{x}', \omega) d\mathbf{x}'
$$

$$
+ \frac{1}{i\omega\rho(\mathbf{x})} \int_{\mathbb{S}_0} \partial_z \hat{F}^*(\mathbf{x}, \mathbf{x}', \omega) \hat{b}(\mathbf{x}', \omega) d\mathbf{x}'. \tag{D.5}
$$

We solve the coefficients $\hat{a}(\mathbf{x}', \omega)$ and $\hat{b}(\mathbf{x}', \omega)$ from the boundary conditions for $\hat{p}(\mathbf{x}, \omega)$ and $\hat{v}_z(\mathbf{x}, \omega)$ at $\mathbb{S}_0$. Choosing $\mathbf{x}$ at $\mathbb{S}_0$ and using Equation (D3), we obtain from Equation (D4)

$$
\hat{p}(\mathbf{x}_H, z_0, \omega) = \hat{a}(\mathbf{x}_H, z_0, \omega) + \hat{b}(\mathbf{x}_H, z_0, \omega). \tag{D.6}
$$

From Equation (D5), we obtain for $\mathbf{x}$ at $\mathbb{S}_0$

$$
\hat{v}_z(\mathbf{x}_H, z_0, \omega) = \frac{1}{i\omega\rho_0} \int_{\mathbb{S}_0} \partial_z \hat{F}(\mathbf{x}, \mathbf{x}', \omega)|_{z=z_0} \hat{a}(\mathbf{x}', \omega) d\mathbf{x}'
$$

$$
+ \frac{1}{i\omega\rho_0} \int_{\mathbb{S}_0} \partial_z \hat{F}^*(\mathbf{x}, \mathbf{x}', \omega)|_{z=z_0} \hat{b}(\mathbf{x}', \omega) d\mathbf{x}'. \tag{D.7}
$$

We define the spatial Fourier transform of $\hat{v}_z(\mathbf{x}_H, z_0, \omega)$ as

$$
\tilde{v}_z(\mathbf{k}_H, z_0, \omega) = \int_{\mathbb{S}_0} \hat{v}_z(\mathbf{x}, \omega) \exp(-i\mathbf{k}_H \cdot \mathbf{x}_H) d\mathbf{x}, \tag{D.8}
$$

where $\mathbf{k}_H = (k_x, k_y)$ (in three dimensions) or $\mathbf{k}_H = k_x$ (in two dimensions). We apply this transformation to both sides of Equation (D7). Since the focusing function is upward propagating at and above $\mathbb{S}_0$ and the medium is homogeneous at and above $\mathbb{S}_0$, we can use the following one-way wave equation for the Fourier transform of the focusing function at $z = z_0$

$$
\partial_z \tilde{F}(\mathbf{k}_H, z, \mathbf{x}'_H, z_0, \omega)|_{z=z_0} = -ik_z \tilde{F}(\mathbf{k}_H, z_0, \mathbf{x}'_H, z_0, \omega), \tag{D.9}
$$

where the vertical wavenumber k_z is defined as

$$
k_z = \begin{cases} \sqrt{\frac{\omega^2}{c_0^2} - \mathbf{k}_H \cdot \mathbf{k}_H}, & \text{for } \mathbf{k}_H \cdot \mathbf{k}_H \leq \frac{\omega^2}{c_0^2}, \\ i\sqrt{\mathbf{k}_H \cdot \mathbf{k}_H - \frac{\omega^2}{c_0^2}}, & \text{for } \mathbf{k}_H \cdot \mathbf{k}_H > \frac{\omega^2}{c_0^2}. \end{cases} \tag{D.10}
$$

The two cases in the latter equation correspond to propagating and evanescent waves, respectively. With this, we obtain for the Fourier transform of Equation (D7)

$$
\tilde{v}_z(\mathbf{k}_H, z_0, \omega) = \frac{-k_z}{\omega\rho_0} \int_{\mathbb{S}_0} \tilde{F}(\mathbf{k}_H, z_0, \mathbf{x}', \omega) \hat{a}(\mathbf{x}', \omega) d\mathbf{x}'
$$

$$
+ \frac{k_z^*}{\omega\rho_0} \int_{\mathbb{S}_0} \tilde{F}^*(-\mathbf{k}_H, z_0, \mathbf{x}', \omega) \hat{b}(\mathbf{x}', \omega) d\mathbf{x}'. \tag{D.11}
$$

Applying the spatial Fourier transformation to Equation (D3), we obtain

$$
\tilde{F}(\mathbf{k}_H, z_0, \mathbf{x}'_H, z_0, \omega) = \exp(-i\mathbf{k}_H \cdot \mathbf{x}'_H). \tag{D.12}
$$

Substituting this into Equation (D11) and using Equation (D8) to define the spatial Fourier transforms of $\hat{a}$ and $\hat{b}$ gives

$$
\tilde{v}_z(\mathbf{k}_H, z_0, \omega) = \frac{-k_z}{\omega\rho_0} \tilde{a}(\mathbf{k}_H, z_0, \omega) + \frac{k_z^*}{\omega\rho_0} \tilde{b}(\mathbf{k}_H, z_0, \omega). \tag{D.13}
$$

Equation (D13) can be combined with the spatial Fourier transform of Equation (D6) into the following matrix–vector equation:

$$
\begin{pmatrix} \tilde{p}(\mathbf{k}_H, z_0, \omega) \\ \tilde{v}_z(\mathbf{k}_H, z_0, \omega) \end{pmatrix} = \begin{pmatrix} 1 & 1 \\ \frac{k_z^*}{\omega\rho_0} & -\frac{k_z}{\omega\rho_0} \end{pmatrix} \begin{pmatrix} \tilde{b}(\mathbf{k}_H, z_0, \omega) \\ \tilde{a}(\mathbf{k}_H, z_0, \omega) \end{pmatrix}. \tag{D.14}
$$

For propagating waves, that is, for $\mathbf{k}_H \cdot \mathbf{k}_H \leq \frac{\omega^2}{c_0^2}$, the vertical wavenumber k_z is real-valued (see Equation D10). Hence, for propagating waves at depth z_0 we may replace k_z^* by k_z in Equation (D14). We then recognize this equation as the well-known expression for wave field composition at depth z_0 (Corones 1975; Ursin 1983; Fishman and McCoy 1984), with $\tilde{b}(\mathbf{k}_H, z_0, \omega) = \tilde{p}^+(\mathbf{k}_H, z_0, \omega)$ and $\tilde{a}(\mathbf{k}_H, z_0, \omega) = \tilde{p}^-(\mathbf{k}_H, z_0, \omega)$, where the superscripts $+$ and $-$ refer to downward and upward propagation. For evanescent waves at depth z_0, that is, for $\mathbf{k}_H \cdot \mathbf{k}_H > \frac{\omega^2}{c_0^2}$, we have $k_z^* = -k_z$; hence, this interpretation of Equation (D14) breaks down. However, assuming evanescent waves are negligible at depth z_0, we may extend the relations $\tilde{b}(\mathbf{k}_H, z_0, \omega) = \tilde{p}^+(\mathbf{k}_H, z_0, \omega)$ and $\tilde{a}(\mathbf{k}_H, z_0, \omega) = \tilde{p}^-(\mathbf{k}_H, z_0, \omega)$ to all $\mathbf{k}_H$. We thus obtain in the space-frequency domain $\hat{b}(\mathbf{x}'_H, z_0, \omega) = \hat{p}^+(\mathbf{x}'_H, z_0, \omega)$ and $\hat{a}(\mathbf{x}'_H, z_0, \omega) = \hat{p}^-(\mathbf{x}'_H, z_0, \omega)$. Substituting this into Equation (D4) yields

$$
\hat{p}(\mathbf{x}, \omega) = \int_{\mathbb{S}_0} \hat{F}(\mathbf{x}, \mathbf{x}', \omega) \hat{p}^-(\mathbf{x}', \omega) d\mathbf{x}'
$$

$$
+ \int_{\mathbb{S}_0} \hat{F}^*(\mathbf{x}, \mathbf{x}', \omega) \hat{p}^+(\mathbf{x}', \omega) d\mathbf{x}', \tag{D.15}
$$

for all $\mathbf{x}$ below the source distribution. Equation (D15) describes extrapolation of the wave field from $\mathbb{S}_0$ to any point $\mathbf{x}$ below the source distribution. Since the source distribution is restricted to the upper half-space, Equation (D15) holds for the entire lower half-space and for a part of the upper half-space below the shallowest source. The lower half-space may in general be inhomogeneous, with propagation velocity $c(\mathbf{x})$ and mass density $\rho(\mathbf{x})$ (we used the one-way wave equation (D9) in the wavenumber–frequency domain only at $\mathbb{S}_0$, where the medium is laterally invariant, to derive that $\hat{a}$ and $\hat{b}$ in Equations (D4) and (D5) can be replaced by $\hat{p}^-$ and $\hat{p}^+$). Finally, transforming Equation (D15) back to the space-time domain yields Equation (23) for all $\mathbf{x}$ below the shallowest source.